ACS OMEGA

Open Access

http://pubs.acs.org/journal/acsodf

Article

Revealing the Preventable Effects of Fu-Zheng-Qu-Xie Decoction against Recurrence and Metastasis of Postoperative Early-Stage Lung Adenocarcinoma Based on Network Pharmacology Coupled with Metabolomics Analysis

Yixi Zhang, Kai Ma, Lei Jiang, Lili Xu, Yingbin Luo, Jianchun Wu,* and Yan Li*

Cite This: *ACS Omega* 2023, 8, 35555−35570

Read Online

ACCESS | Metrics & More | Article Recommendations | Supporting Information

ABSTRACT: Fu-Zheng-Qu-Xie (FZQX) decoction is a traditional Chinese herbal prescription for the treatment of lung cancer and exerts proapoptotic and immunomodulatory effects. It has been clinically suggested to be effective in improving the survival of postoperative early-stage lung adenocarcinoma (LUAD), but the mechanism remains unclear. In this study, we used network pharmacology coupled with metabolomics approaches to explore the pharmacological action and effective mechanism of FZQX against the recurrence and metastasis of postoperative early-stage LUAD. Network pharmacology analysis showed that FZQX could prevent the recurrence and metastasis of postoperative early-stage LUAD by regulating a series of targets involving vascular endothelial growth factor receptor 2, estrogen receptor 1, sarcoma gene, epidermal growth factor receptor, and protein kinase B and by influencing the Ras, PI3K-Akt, and mitogen-activated protein kinase signaling pathways. In liquid chromatography−mass spectrometry analysis, 11 differentially expressed metabolites, including PA(12:0/18:4(6Z,9Z,12Z,15Z)), PC(16:0/0:0)[U], LysoPC(18:1(11Z)), and LysoPC(18:0), were discovered in the FZQX-treated group compared to those in the model group before treatment or normal group. They were enriched in cancer metabolism-related signaling pathways such as central carbon metabolism in cancer, choline metabolism, and glycerol phospholipid metabolism. Collectively, our results suggest that the multicomponent and multitarget interaction network of FZQX inhibits the recurrence and metastasis of postoperative early-stage LUAD by activating the receptor signal transduction pathway to inhibit proliferation, induce cell apoptosis, inhibit aerobic glycolysis, and reprogram tumor lipid metabolism.

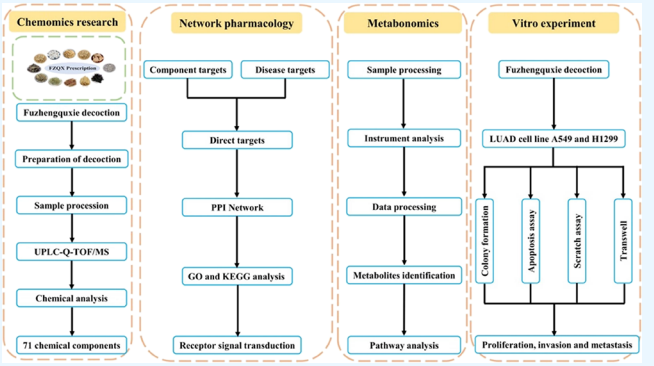

1. INTRODUCTION

Lung cancer is one of the most common malignant tumors with a high incidence rate and high mortality rate. There were more than 2.2 million new lung cancers and 1.8 million deaths in 2020, which poses a serious threat to human health according to the latest global cancer burden data from the International Agency for Research on Cancer (IARC) of the World Health Organization.[1] Lung adenocarcinoma (LUAD) is a subtype of lung cancer accounting for 40−50% of total lung cancer cases, and the incidence rate and mortality rate are increasing yearly.[2] Although early-stage LUAD generally has no obvious clinical symptoms, hematogenous metastasis also occurs in early-stage LUAD, which directly affects the survival prognosis of patients.[3,4] Early-stage LUAD patients are usually treated with complete surgical resection, while postoperative recurrence and metastasis are still the most important factors related to the survival of LUAD patients.[5] According to the postoperative pathological type and degree of lymphatic metastasis, some stage IB LUAD patients still need adjuvant chemotherapy after surgery.[6] However, the benefits of postoperative adjuvant chemotherapy in stage IB LUAD patients are still under debate, and side effects represent a significant threat to quality of life.[7] Thus, strategies to prolong the survival of postoperative patients with early-stage LUAD are urgently needed to improve outcomes in patients with this disease.

In recent years, traditional Chinese medicine (TCM) has attracted considerable attention as a candidate anticancer alternative drug owing to its clinically proven anticancer efficacy and relatively low toxicity.[8,9] After long-term clinical practice,

Received: January 7, 2023
Accepted: June 27, 2023
Published: September 20, 2023

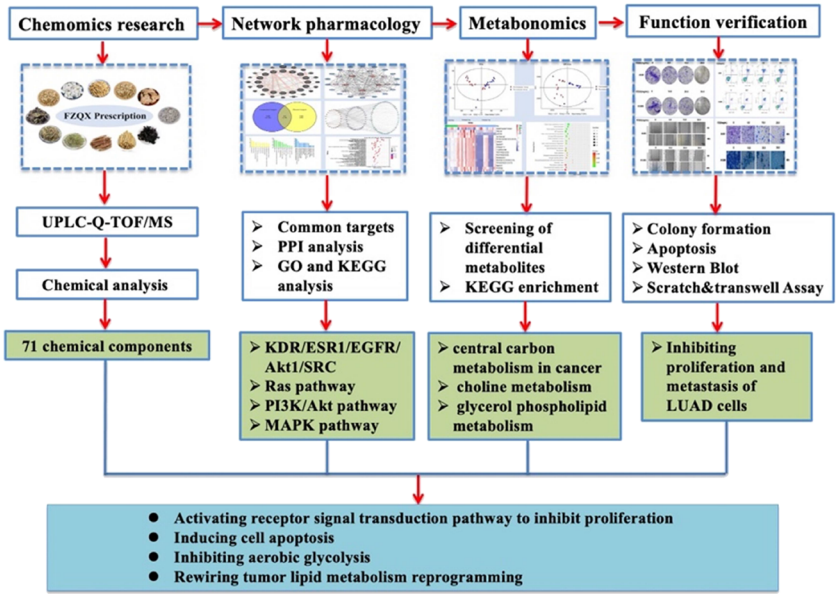

Figure 1. Flow chart for the study.

Chinese herbal Fu-Zheng-Qu-Xie (FZQX) prescription, as adjuvant therapy for postoperative lung cancer, has been proven to be effective in many studies. The results of previous research showed that FZQX has an obvious antirecurrence effect, which not only prolongs the median progression-free time of lung cancer patients but also alleviates symptoms and reduces the side effects caused by chemotherapy.[10,11] FZQX consists of 12 commonly used Chinese herbs, including *Astragalus membranaceus* (Fisch.) Bunge (Huang-Qi), *Glehnia littoralis Fr. Schmidt* (Bei-Sha-Sheng), *Ophiopogon japonicus* (L.f) Ker-Gawl (Mai-Dong), *Atractylodes macrocephala Koidz* (Bai-Zhu), *Poria cocos* (Bai-Fu-Ling), *Codonopsis pilosula* (Franch.) Nannf. (Dang-Shen), *Selaginella doederleinii* Hieron (Shi-Shang-Bai), *Salvia chinensis Benth* (Shi-Jian-Chuan), *Solanum septemlobum Bunge* (Shu-Yang-Quan), *Prunella vulgaris* L. (Xia-Ku-Cao), *Sargassum pallidum* (Turn.) C.Ag. (Hai-Zao), and *Ostrea gigas Thunberg* (Mu-Li). An increasing number of studies have shed light on how single drugs and bioactive ingredients within FZQX exert anti-LUAD effects.[12−14] Modern pharmacology research has shown that Ophiopogon B, the active ingredient of *O. japonicus*, can inhibit the metastasis and angiogenesis of LUAD A549 cells by regulating the EphA2/Akt signaling pathway.[15] A recent study showed that the *P. cocos* active ingredient could exert cytotoxicity on human LUAD cells by inducing mitochondrial apoptosis.[16] Another study reported that *P. vulgaris polysaccharide* could reshape the tumor immune microenvironment by increasing the thymus index and spleen index in LUAD tumor-bearing mice.[17] However, the components of Chinese herbal prescriptions are complex and characterized by multitargets, multiple effects, and multiple pathways, and a single drug cannot represent and predict a compound drug system containing hundreds of chemical components. Currently, the overall mechanism of action of FZQX is not well understood, so designing a strategy for exploring the potential mechanism of FZQX against the recurrence of LUAD paves the way for future research.

Scientific and technological progress has accelerated the continuous development of cancer research, bioinformatics technology, and omics research, providing data support for the study of the integral mechanism between drugs and diseases.[18] Network pharmacology is a research method based on the combination of pharmacology and systems biology that can comprehensively and systematically predict the links between chemical constituents, target proteins, and pathways of TCM and is widely used in TCM research.[19] Mass spectrometry (MS) technology plays a critical role in the research field of TCM owing to its high separation ability, high selectivity, high sensitivity, and ability to provide molecular weight and structure information for complex samples.[20] Yi et al. conducted a comprehensive metabolomics and pharmacokinetics study of the herbal medicine *Saussurea laniceps* Hand.-Mazz. (SL) based on the UPLC-DAD-QTOF-MS technique, and this research strategy improved both the precision of quantitative analysis for metabolomic studies and the accuracy of quantitative analysis for pharmacokinetic studies, making the study of Chinese medicine more efficient.[21] At the same time, the research team used UPLC-DAD-QTOF-MS technology to analyze the species and evaluate the overall quality of *Saussurea involucrata* from three different sources. The results of this study standardized the quality of multisource medicinal plants and allowed the regulation of Chinese medicine counterfeiting.[22] Tang et al. used UPLC-QTOF-MS to compare the metabolic characteristics of the active ingredient saponin in the herbal medicine *Dioscorea opposita*, and further demonstrated the sustained level of metabolites in rat biological samples after oral administration of *D. opposita*.[23] In addition, Feng et al. found that the Chinese herbal medicine *D. opposita* could exert therapeutic effects on myocardial ischemia by increasing the level of enzymatic and nonenzymatic antioxidants in vivo, reducing oxidative stress damage and metabolic markers related to intestinal flora metabolism by the UPLC−MS technique.[24] Metabonomics, a branch technology of systems biology, is a promising strategy to seize the metabolic alterations of endogenous metabolites through multivariate analysis and reveal the intervention mechanism of TCM. The metabonomics method will become an essential tool for uncovering disease pathogenesis and mechanisms of multicomponent medicinal effects.[25] Currently, the comprehensive research strategy of combining the integrity and systematic characteristics of network pharmacology with the high sensitivity of metabonomics has successfully revealed the

https://doi.org/10.1021/acsomega.3c00122
ACS Omega 2023, 8, 35555−35570

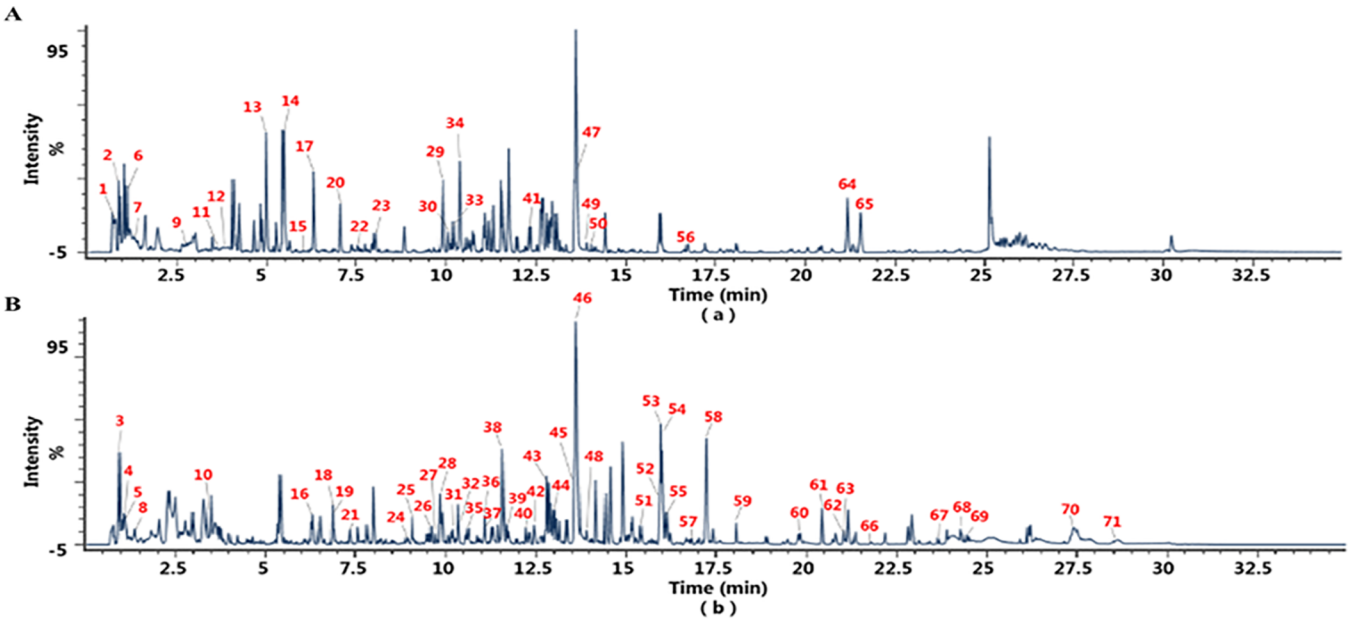

Figure 2. Base peak chromatogram of the FZQX prescription based on UPLC-Q-TOF/MS. (A) Base peak chromatogram of FZQX prescription in the positive mode and (B) base peak chromatogram of FZQX prescription in the negative mode.

mechanisms of TCM prescriptions. The research strategy conforms to the characteristics of multicomponent, multitarget, and multipathway treatment of TCM.[26−28] Thus, the combination of multiomics research methods addresses an unmet need for revealing the mechanism of TCM and detecting disease-related targets.

Based on the above research status, we used network pharmacology coupled with metabonomics analysis to reveal the mechanism of FZQX against the recurrence and metastasis of postoperative early-stage LUAD. To identify the relevant target and pathway of postoperative early-stage LUAD after FZQX treatment, a "compound-target-pathway" interaction network was established through network pharmacology. Moreover, metabonomics analysis was applied to explore differential metabolites, thus providing the metabolic mechanism of FZQX in treating postoperative early-stage LUAD. Our results suggest that FZQX prevents the recurrence and metastasis of postoperative early-stage LUAD by activating the receptor signal transduction pathway to inhibit proliferation, induce cell apoptosis, inhibit aerobic glycolysis, and reprogram tumor lipid metabolism. The overall flowchart for elucidating the mechanism of FZQX in the treatment of postoperative early-stage LUAD is illustrated in Figure 1.

2. RESULTS

2.1. Identification of FZQX Prescription Components. The components of the FZQX prescription were qualified by HPLC-Q-TOF-MS/MS analysis according to the conditions in Section 5.1.2. As shown in Figure 2A,B, the total ion chromatogram (TIC) included 25 compounds in the positive mode and 46 compounds in the negative mode. Through retention times of main chromatographic peaks, measured value, adduct ion, generated fragment ion information of the secondary mass spectrum, and along with analysis of the information obtained from the literature sources and reference standard, a total of 71 chemical constituents in the FZQX prescription were characterized, including 6 amino acid compounds, 27 phenolic compounds, 8 organic compounds, 13 terpene compounds, 1 quinone compound, 1 nucleoside compound, 1 cinnamic acid compound, 1 vitamin compound, 1 aromatic compound, and 12 of other classes (see Table 1).

2.2. Analysis of the Antitumor Mechanism of FZQX Prescription on Postoperative Early-Stage LUAD by Network Pharmacology Approach. *2.2.1. Establishment of the Chemical Components Library of FZQX Prescription and Target Prediction.* According to analysis and comparison, a total of 71 chemical components were identified. To collect component targets of FZQX prescriptions, we used the TCMSP database, and a total of 166 targets of 64 chemical components were retrieved. The SDF document with 37 components of the 2D structure obtained in the PubChem database was imported into Swiss Target Prediction. After removing the duplicated parts, 171 chemical constituents were accepted, and their structures were retrieved from the PubChem database. Then, they were transformed into standard gene targets by the UniProt database (see Supplementary Table S1).

2.2.2. Acquisition of the Targets of FZQX Prescription in Preventing the Recurrence of Postoperative Early-Stage LUAD. To acquire "disease targets," we used "postoperative early-stage LUAD" as the keyword, and 182 disease targets were found in GeneCards (see Supplementary Table S2). The 150 chemical composition-related targets and 166 disease targets obtained from Sections 5.2.2.1 and 5.2.2.2 were uploaded to draw a Venn diagram for analysis, and 16 common targets were obtained (see Figure 3A). A total of 16 common targets obtained from Section 5.2.2.3 were uploaded to Gene MANIA. The source type was set as "*Homo sapiens*", and 20 indirect targets were analyzed (see Figure 3B).

2.2.3. Construction and Analysis of Protein−Protein Interaction Network. Thirty-six targets were imported into the String database, and the protein interaction relationship was obtained. Cytoscape 3.7.2 software for visualization was imported, and a total of 35 nodes and 202 edges were involved. We were surprised to see AKT1, ESR1, KDR, SRC, and EGFR at the center of the network (see Figure 3C).

https://doi.org/10.1021/acsomega.3c00122
ACS Omega 2023, 8, 35555−35570

Table 1. Identification of Chemical Components of the FZQX Prescription[a]

no.	identification status	observed *m/z*	mass error (mDa)	observed RT (min)	theoretical fragments found	adducts	TCM
1	3-methoxy-4-hydroxybenzoic acid	151.0346	−4.3	0.7	0	$-H_2O$ + H	DS/MD/HZ
2	arginine	175.1185	−0.4	0.87	2	+H, +Na	BSS/BZ/DS/HQ
3	pentose	195.0509	−0.1	0.95	1	+HCOO, $-H_2O$ + HCOO	HQ/BZ/DS/BFL/BSS/SJC/SSB/MD/SYQ/HZ/XKC
4	hesperidin	609.1873	4.9	1.07	24	−H	SJC/SYQ
5	coreline C	533.1713	4.8	1.08	12	$-H_2O$-H	DS
6	proline	138.0543	1.7	1.08	1	+Na, +H	BZ/DS/HQ/MD/SYQ
7	methyl ophiopogon flavanone A	365.1039	4.3	1.3	0	+Na	BZ
8	shikimic acid	173.0455	0	1.56	2	−H, $-H_2O$-H	SSB
9	glutamate	130.0493	−0.5	2.76	1	$-H_2O$ + H	BSS/DS/MD/SJC/SSB/SYQ
10	*β*-uridine	243.0622	−0.1	3.4	3	−H	BZ
11	methyl ophiopogon flavanone A isomer	325.1117	4.6	3.51	1	$-H_2O$ + H	MD
12	methyl ophiopogon flavanone A isomer	325.1116	4.5	3.75	1	$-H_2O$ + H	BZ
13	hordenine-*O*-*α*-L-rhamnoside	312.1799	−0.6	4.98	7	+H	SSB
14	codonopsis	268.1543	0	5.45	4	+H	DS
15	secoisolariciresinol	367.1487	−2.9	6.11	0	$-H_2O$ + Na	BSS/DS
16	chlorogenic acid	353.0881	0.3	6.26	2	−H	XKC
17	tryptophan	205.0967	−0.4	6.29	9	+H	BSS/DS/HQ/MD
18	vitamin B1	299.0777	3.8	6.88	1	−H	HQ
19	macrophyllin	137.0248	0.4	6.89	2	$-H_2O$-H	SYQ/HQ
20	falcarindiol	265.1547	−1.6	7.03	5	$-H_2O$ + Na	SYQ
21	chlorogenic acid	353.0872	−0.6	7.33	4	−H	XKC/BZ
22	swertimarin	357.1173	−0.7	7.53	7	$-H_2O$ + H	SJC/SYQ
23	*cis*-caffeic acid	163.0385	−0.5	8	2	$-H_2O$ + H, +H	SJC/SYQ/XKC
24	codonopsis glycoside I	677.2293	−0.5	8.94	3	−H	DS
25	salvianolic acid D	463.0915	3.3	9.06	6	+HCOO, −H	XKC
26	poriol	331.0819	−0.4	9.59	5	+HCOO	SJC
27	rutin isomer	609.1461	0	9.76	1	-H	SYQ
28	rutin isomer	609.1457	−0.4	9.85	7	−H	SJC/SYQ/XKC
29	3′-methoxy-5′-hydroxyisoflavone-7-*O*-*β*-D-glucoside	447.128	−0.5	9.9	6	+H, +Na	HQ
30	6-methoxy-7-hydroxycoumarin	193.049	−0.5	10.14	0	+H	BSS/SYQ
31	chlorogenic acid	353.0876	−0.2	10.16	3	−H	SSB
32	salvianolic acid D	463.0878	−0.4	10.19	9	+HCOO	SYQ
33	isoquercetin	465.1018	−0.9	10.2	5	+H	SJC/XKC
34	*cis*-caffeic acid	163.0385	−0.5	10.33	3	$-H_2O$ + H	XKC
35	selaginin B	521.2024	−0.5	10.61	10	$-H_2O$-H, $-H_2O$ + HCOO	SSB
36	calycosin	283.0609	−0.3	11.28	7	−H	HQ
37	salvianolic acid B isomer	717.1436	−2.5	11.32	14	−H	SYQ
38	rosmarinic acid	359.0767	−0.6	11.56	21	−H	SYQ
39	salvianolic acid A	493.1125	−1.6	11.67	11	−H	SJC
40	salvianolic acid B isomer	717.144	−2.1	12.21	14	−H	SJC
41	4′-hydroxyimperatorin-4′-*O*-*β*-D-pyranoglucoside	431.1327	−1	12.32	10	$-H_2O$ + H, $-H_2O$ + Na	HQ
42	sericoside	711.3952	−0.9	12.44	4	+HCOO	SJC/SYQ
43	borneol-2-*O*-*β*-D-celery-(1_6) -*β*-D-glucoside	493.2278	−1.2	12.73	0	+HCOO	MD
44	9,10-dimethoxy sandalwood-3-*O*-*β*-D-glucoside	507.1511	0.3	13.05	30	+HCOO	HQ
45	poriol	267.0663	0.1	13.55	4	$-H_2O$-H	HQ
46	14-hydroxy sprengerinin C isomer	915.4586	−0.9	13.61	51	+HCOO, $-H_2O$ + HCOO	XKC
47	calycosin	285.0752	−0.6	13.65	2	+H	HQ
48	*Ophiopogon japonicus* saponins E	769.4003	−1.3	13.89	6	+HCOO	XKC
49	*Lycium barbarum* C	964.4177	0.2	13.92	25	+Na	SSB/SYQ
50	quercetin-3-methyl ether	339.0484	0.9	14.14	3	+Na, $-H_2O$ + Na	XKC
51	astragaloside A	695.4006	−0.6	15.37	5	+HCOO	SJC
52	dehydrotumulosic acid	529.3527	−0.8	15.9	1	+HCOO	BFL
53	14-sydroxy sprengerinin C isomer	897.4459	−3	15.96	16	$-H_2O$ + HCOO	XKC

https://doi.org/10.1021/acsomega.3c00122
ACS Omega 2023, 8, 35555−35570

Table 1. continued

no.	identification status	observed *m/z*	mass error (mDa)	observed RT (min)	theoretical fragments found	adducts	TCM
54	tianshic acidisomer	329.2329	−0.4	16	7	−H	SJC/SSB/SYQ/XKC/BFL/DS/HQ
55	tianshic acidisomer	329.2326	−0.7	16.11	4	−H	XKC/BFL/DS
56	poriol	269.0801	−0.7	16.72	1	$-H_2O$ + H	HQ
57	astragaloside IV	829.4565	−2.6	16.95	4	+HCOO	HQ
58	tianshic acidisomer	329.2327	−0.7	17.21	5	−H	XKC
59	astragaloside II	871.4683	−1.4	18.05	2	+HCOO	HQ
60	poricoic acid DM	555.3312	−1.5	19.84	1	$-H_2O$ + HCOO	SYQ/DS/HQ
61	isoastragaloside I	913.4796	−0.7	20.43	3	+HCOO	HQ
62	asparagin B	749.4108	−1	21.02	1	$-H_2O$ + HCOO	SYQ
63	25-hydroxyporicoic acid H	497.3265	−0.8	21.09	1	$-H_2O$-H	BFL
64	3*β*-hydroxyapatrone isomer	215.1422	−0.9	21.17	23	$-H_2O$ + H, +H	SJC
65	3*β*-hydroxyapatrone isomer	215.1423	−0.8	21.54	27	$-H_2O$ + H, +H	SJC
66	sprengerinin C	899.4641	−0.5	21.64	1	+HCOO	MD
67	asparagin B	941.4754	0.3	23.65	0	+HCOO	MD
68	26-hydroxyporicoic acid DM	589.3379	−0.3	24.27	3	+HCOO	XKC
69	3-*O*-acetyl-16*α*-hydroxy-dehydrotrametenolic acid	539.335	−2.8	24.43	1	$-H_2O$ + HCOO	SYQ
70	tanshinone diphenol	297.1532	3.6	27.43	1	−H	HZ/ML/SYQ
71	ergosterol	423.3272	0.3	28.98	1	$-H_2O$ + HCOO	BFL

[a]Abbreviation: HQ (Huang-Qi): *Astragalus membranaceus* (Fisch.) Bge. Var. mongholicus (Bge.) Hsiao; BZ (Bai-Zhu): *Atractylodes macrocephala* Koidz.; MD (Mai-Dong): *Ophiopogon japonicus* (L.f) Ker-Gawl.; BSS (Bei-Sha-Shen): *Glehnia littoralis* Fr. Schnidt; Poria (Bai-Fu-Ling): *Poria cocos* (Schw.) Wolf.; Codonopsis Radix (Dang-Shen): *Codonopsis pilosula* (Franch.) Nannf. and *Codonopsis pilosula* Nannf. var. Modesta (Nannf.) L. T. Shen and *Codonopsis tangshen* Oliv.; SSB (Shi-Shang-Bai): *Selaginella doederleinii* Hieron.; SJC (Shi-Jian-Chuan): *Salvia chinensis* Benth.; SYQ (Shu-Yang-Quan): *Solanum septemlobum* Bunge; XKC (Xia-Ku-Cao): *Prunella vulgaris* L.; HZ (Hai-Zao): *Sargassum pallidum* (Turn.) C.Ag. and *Sargassum fusiforme* (Harv.) Setch.; and ML (Mu-Li): *Ostreae gigas* Thunberg. and *Ostrea talienwhanensis* Crosse. and *Ostrea rivularis* Gould.

2.2.4. GO and KEGG Pathway Enrichment Analysis. The targets were integrated and imported into the String database, and the TSV format file was saved. The targets were obtained, including 486 biological processes ("enzyme-linked receptor protein signaling pathway," "transmembrane receptor protein tyrosine kinase signaling pathway," "positive regulation of intracellular signal transduction," etc.), 12 cellular components ("receptor complex," "plasma membrane," "phosphatidylinositol 3-kinase complex," etc.), 63 molecular functions ("protein binding," "transmembrane receptor protein tyrosine kinase activity," "enzyme binding," etc.), and 114 KEGG pathways (see Figure 3D). Moreover, the top 50 enriched KEGG pathways are displayed in Figure 3E, including those for the Ras signaling pathway, PI3K-Akt signaling pathway, and MAPK signaling pathway.

2.2.5. Construction of "Chemical Component-Target-Pathway". To intuitively show the relationship between 24 active ingredients and 34 action targets and 49 KEGG pathways, we used Cytoscape 3.7.2 software to establish a "chemical component-target-pathway" network model (see Figure 3F). Meanwhile, we found that the same component corresponds to multiple action targets, and multiple action targets correspond to the same pathway.

2.3. Metabolomic Study of FZQX Prescription in Preventing Recurrence of Postoperative Early-Stage LUAD. *2.3.1. QC Sample Analysis.* We took the same amount of serum samples from all patients and mixed them as QC samples. In the MS process, one QC sample was inserted into every 10 official samples, and the QC sample was used to evaluate the stability of the MS platform system during the whole experimental process. To explore the metabolomic effects of pretreatment vs control groups and posttreatment vs pretreatment groups, PCA and OPLS-DA analyses were performed. PCA showed samples separated in the score plots, indicating significant differences in the distribution of endogenous metabolites in the pretreatment and posttreatment groups (see Figure 4A). OPLS-DA also indicated that the serum metabolites in the posttreatment vs pretreatment groups were well separated, suggesting that FZQX prescription interfered with the metabolic spectrum of postoperative early-stage LUAD patients (see Figure 4B). Figure 4C evaluated whether the OPLS-DA model was overfitted by using 7-fold cross-validation and 200 response permutation testing (RPT). Q2 values <1 were carried out to assess the predictability of the model, indicating good data quality, and reproducibility of the analytical methods.

2.3.2. Identification of Differential Metabolites. OPLS-DA was constructed to select significant variables, and variables were selected as potential biomarkers when their VIP values were larger than 1.0 and the absolute values of their *p* were greater than or equal to 0.5. HMDB websites were also used for metabolite identification. To investigate similarities and differences between significant metabolites in three different groups, Venn diagrams were established. The results showed that 229 (pretreatment vs control) and 365 (posttreatment vs pretreatment) differential metabolites were acquired (see Supplementary Tables S3 and S4), and a total of 89 differential variables were merged (see Figure 4D). To more intuitively compare the metabolite differences between the control group, the pretreatment group and the posttreatment group, a heatmap of the differential biomarkers was generated based on their relative abundance (see Figure 4E). Compared with the control group, the relative expression of metabolites of the preadministration group, including PS(18:1(9Z)/20:5(5Z,8Z,11Z,14Z,17Z), PS-(17:2(9Z,12Z)/22:6(4Z,7Z,10Z,13Z,16Z,19Z)), PA(12:0/18:4(6Z,9Z,12Z,15Z)), PS(15:0/18:4(6Z,9Z,12Z,15Z)), PC-(16:0/0:0)[U], LysoPC(18:1(11Z)), and LysoPC (18:0), were significantly upregulated. In contrast, these differential metab-

https://doi.org/10.1021/acsomega.3c00122
ACS Omega 2023, 8, 35555−35570

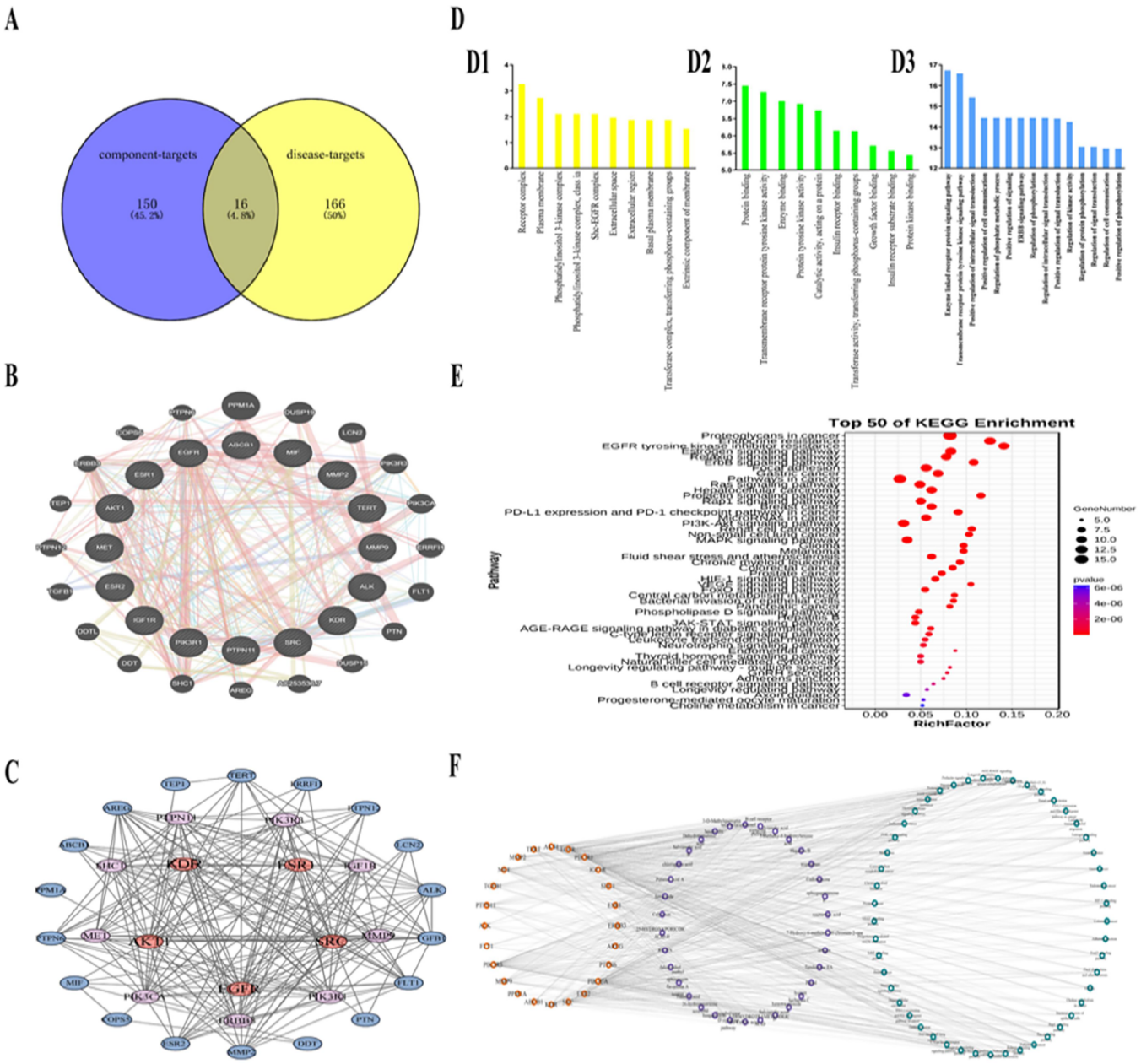

Figure 3. Network pharmacology analysis of the modulatory effect of FZQX prescription on postoperative early-stage LUAD. (A) Venn diagram of targets of FZQX prescription and postoperative early-stage LUAD. Among them, the purple circle suggests that there are 166 chemical composition targets of FZQX, the yellow circle indicates 182 postoperative early-stage LUAD targets, and the middle crossing part indicates 16 "common targets." (B) "Indirect targets" of FZQX prescription. Target map of FZQX in the treatment of postoperative early-stage LUAD. Among them, the nodes on the inner circle represent 16 common targets of FZQX in the treatment of postoperative early-stage LUAD, and the nodes on the outer circle represent 20 indirect targets of FZQX in the treatment of postoperative early-stage LUAD. (C) PPI network diagram of FZQX prescription-related postoperative early-stage LUAD targets. In the figure, the node represents the target protein, the edge represents the interaction between the target protein, the size and color of the node represent the degree value, and the color of the edge represents the combined score value. (D) GO function enrichment analysis, (D1) cellular components involved in the target, (D2) molecular functions involved in the target, and (D3) biological process involved in the target. (E) KEGG enrichment analysis of the predicted targets of FZQX for the treatment of postoperative early-stage LUAD. Dot plot showing the top 50 KEGG pathways: the size of the dots corresponds to the number of genes annotated in the entry, and the color of the dots corresponds to the corrected P value. (F) Network diagram of "composition-disease-pathway-target" of FZQX prescription. Orange nodes represent chemical components, purple nodes represent disease targets, and green nodes represent pathways.

olites showed a clear downward trend after FZQX prescription treatment, suggesting that they can be used as potential biomarkers for FZQX prescription treatment of LUAD.

2.3.3. Metabolic Pathway Analysis. Compared with the control group, 7 corresponding metabolic pathways are displayed in Figure 4F, including those for protein absorption and decomposition, biosynthesis of valine, leucine and isoleucine biosynthesis, ABC transporters, mineral absorption, glycosylphosphatidylinositol (GPI)-anchor biosynthesis, autophagy, and cancer central carbon metabolism. As shown in Figure F2, the top three pathways, including cancer center carbon metabolism, protein absorption and decomposition, and

https://doi.org/10.1021/acsomega.3c00122
ACS Omega 2023, 8, 35555−35570

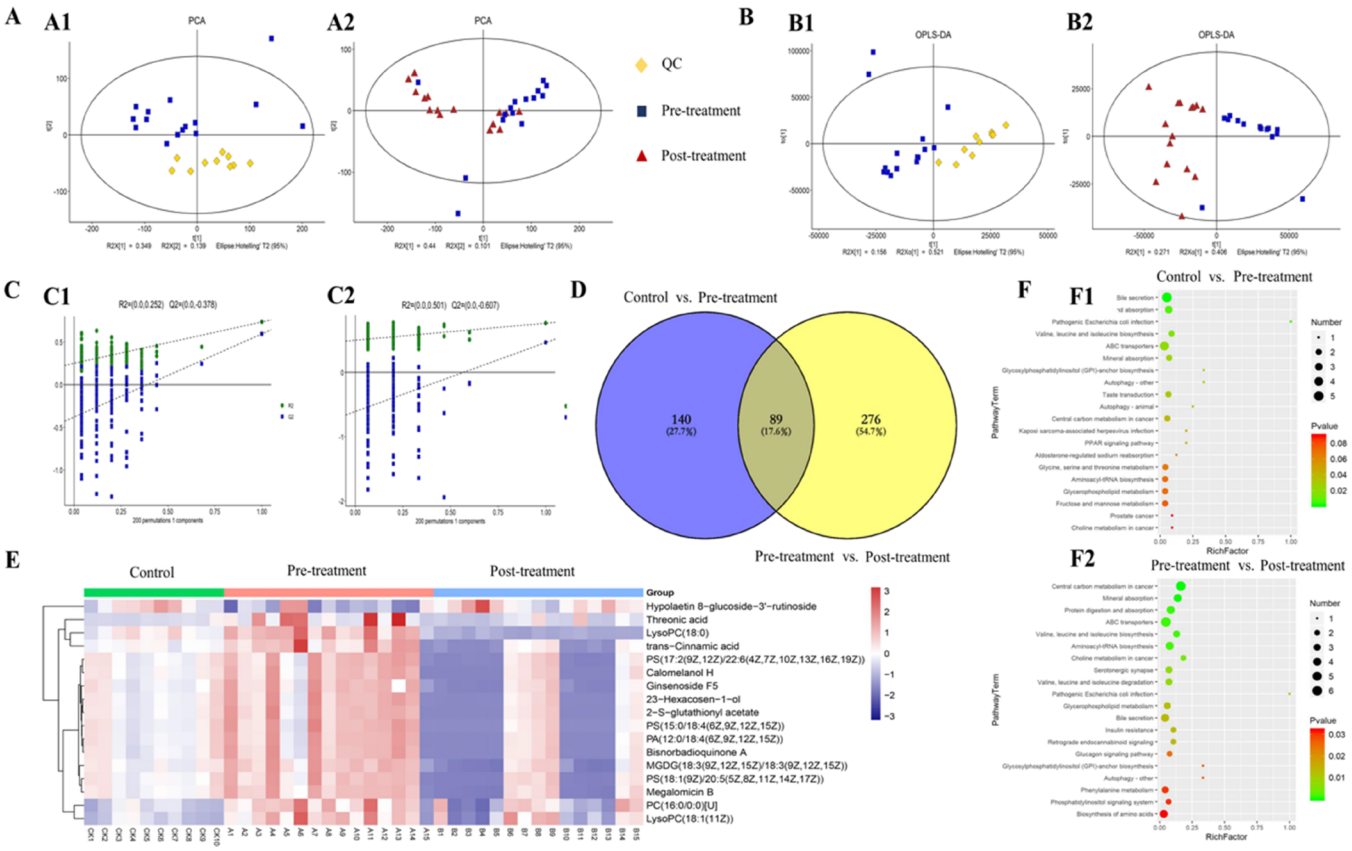

Figure 4. Metabolomic profile analysis of FZQX prescription against postoperative early-stage LUAD. (A) PCA score plots obtained from the control, pretreatment, and posttreatment groups, (A1) PCA score plots in the control vs pretreatment, R2 = 0.349, R2 = 0.139, (A2) in the pretreatment vs posttreatment, R2 = 0.44, R2 = 0.101. Yellow, blue, and red marks were labeled as the control, pretreatment, and posttreatment groups, respectively, (B) OPLS-DA score plots obtained from the control, pretreatment and posttreatment groups, (B1) OPLS-DA score plots in the control vs pretreatment, R2 = 0.156, R2 = 0.521, (B2) in the pretreatment vs posttreatment, R2 = 0.271, R2 = 0.406. Yellow, blue, and red marks were labeled as the control, pretreatment, and posttreatment groups, respectively. (C1 and C2) Permutation tests in the control vs pretreatment and pretreatment vs posttreatment groups showed that the OPLS-DA model was reliable. (D) Venn diagram of metabolites showing the similarities and differences between the control, pretreatment and posttreatment groups. Among them, the purple circle indicates that there are 229 differential metabolites in the control vs pretreatment group, the yellow circle presents 365 differential metabolites in the pretreatment vs posttreatment group, and the middle crossing part suggests 89 differential metabolites. (E) Heatmap visualizing the changes in the contents of differential metabolites in the control, pretreatment and posttreatment groups. (F1 and F2) KEGG pathway enrichment analysis of differential metabolites in the control vs pretreatment group and pretreatment vs posttreatment group.

mineral absorption, played an important role in regulating the postoperative early stage after FZQX administration. Therefore, we can confirm that FZQX prescription has a potential influence on glucose metabolism, amino acid metabolism, and choline metabolism.

2.4. FZQX Prescription Inhibits Proliferation and Metastasis of LUAD Cells In Vitro. Two LUAD cell lines (A549 and H1299) were selected to investigate the effect of FZQX on the proliferation and metastasis of LUAD cells. First, a CCK-8 assay was used to detect the effect of FZQX on the viability of A549 and H1299 LUAD cells. As shown in Figure 5A, the IC_{50} values of A549 and H1299 cells were 7.98 and 9.79 mg/mL, respectively. Subsequently, we conducted a CCK-8 assay in BEAS-2B cells using an FZQX concentration of 12 mg/mL. The results showed that FZQX exerted cytotoxic effects in a dose-dependent manner, and a high concentration of FZQX did not significantly inhibit normal human lung epithelial cells. Colony formation assays were used to analyze the inhibitory effects of FZQX, and we found that the efficiency of colony formation decreased with FZQX treatment in a dose-dependent manner ($p < 0.05$, $p < 0.01$, see Figure 5B). To illuminate the underlying mechanism by which FZQX curtailed cancer cell growth, we performed apoptosis assays. The results showed that 6 and 10 mg/mL FZQX treatment elicited a time course of cell apoptosis in A549 and H1299 cells ($p < 0.05$, see Figure 5C), indicating that FZQX impaired cancer cell growth by inducing cell apoptosis. The expression of the well-known cell proliferation markers proliferating cell nuclear antigen (PCNA) and Ki67 consistently started to decrease with different doses of FZQX treatment in A549 cells and H1299 cells, while the expression of the well-known cell apoptosis markers BCL2-associated X (Bax) and B-cell lymphoma-2 (Bcl-2) consistently started to increase and decrease, respectively, with different doses of FZQX treatment ($p < 0.05$, $p < 0.01$, see Figure 5D). Collectively, these in vitro experimental data demonstrated the inhibitory effect of FZQX on cancer cell growth over a long treatment period. Wound healing assays and Transwell assays were used to analyze the effects of cell migration and invasion. The results of the wound healing assay confirmed that the migration ability of cells after treatment with different concentrations of FZQX was decreased in comparison with that of the control group in a concentration-dependent manner, and the differences were

https://doi.org/10.1021/acsomega.3c00122
ACS Omega 2023, 8, 35555−35570

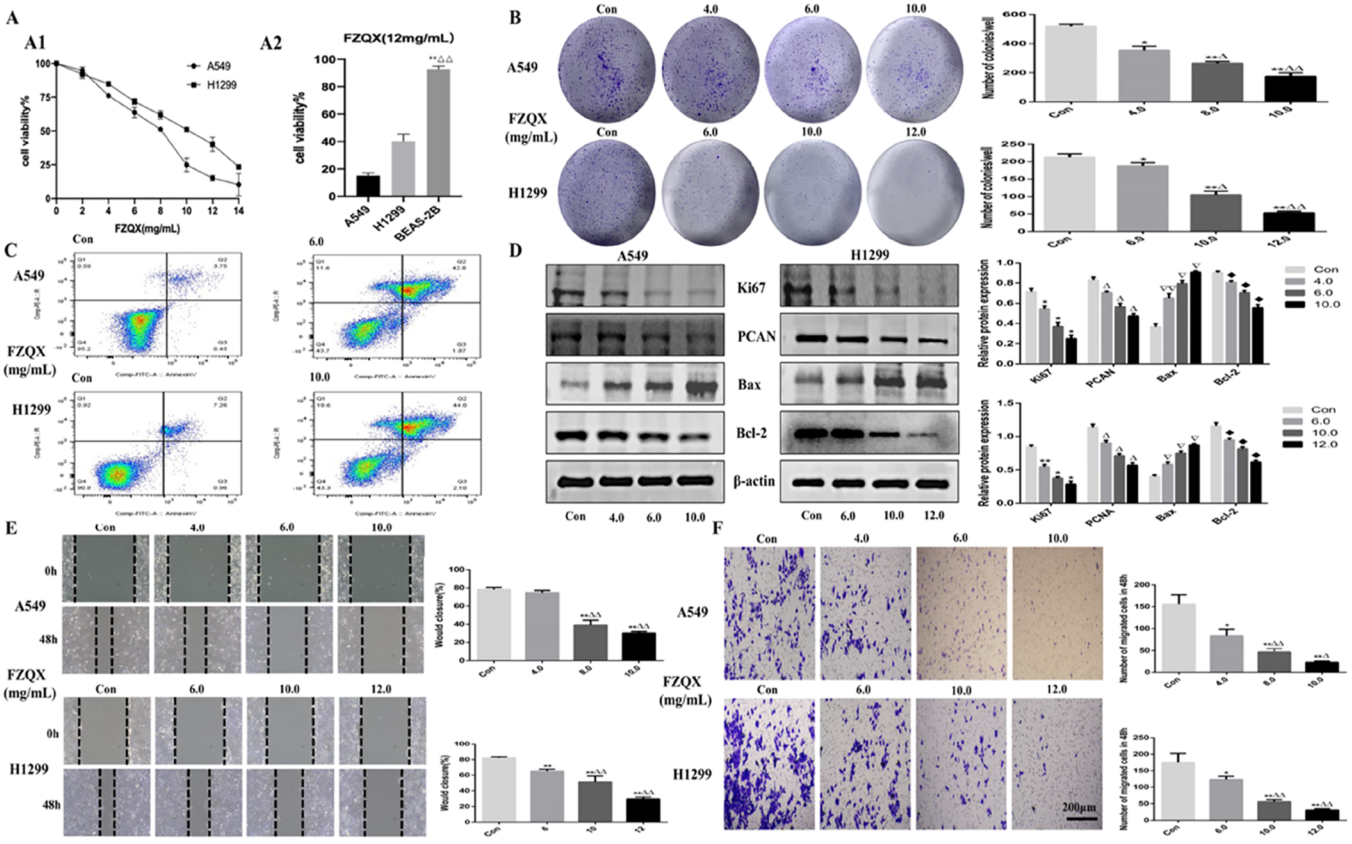

Figure 5. FZQX treatment inhibited the proliferation and migration of LUAD cells. (A) Effects of FZQX prescription on the proliferation of A459 and H1299 cells determined by CCK-8 assay, (A1) LUAD cells (A549 and H1299) were treated with different concentrations of FZQX prescription for up to 48 h to examine the cell viability, (A2) A549, H1299, and BEAS-2B were treated with high-dose concentration (12 mg/mL) for up to 48 h to examine the cell viability. (B) A549 and H1299 cells were treated with different concentrations of FZQX prescription for 14 days to examine the colony formation abilities. (C) Representative results of the apoptosis analyses by FACS. FZQX prescription induced cell apoptosis in A459 and H1299 cells. (D) Different concentrations of FZQX prescription decreased Ki67, PCNA, and Bcl-2 but increased Bax expression in both H1299 and A549 cell lines. (E) Representative results of scratch assays in different concentrations of FZQX-treated A549 and H1299 cells at 48 h. (F) Representative results of Transwell migration assays in different concentrations of FZQX-treated A549 and H1299 cells at 48 h. The mean ± SD was calculated for all experimental values. * and ** indicate a statistically significant difference compared to the control group ($p < 0.05$ and $p < 0.01$, respectively). △ and △△ indicate a statistically significant difference compared to different concentrations of the FZQX group ($p < 0.05$, $p < 0.01$, respectively).

statistically significant ($p < 0.05$, $p < 0.01$, see Figure 5E). Moreover, the outcome of the Transwell assay was consistent with the wound healing assay results ($p < 0.05$, $p < 0.01$, see Figure 5F).

3. DISCUSSION

3.1. FZQX Inhibits the Proliferation and Metastasis of LUAD Cells In Vitro. Early-stage LUAD has a high incidence and complicated pathogenesis; in particular, micropapillary LUAD is at high risk of metastasis.[29] The discovery of circulating tumor cells reveals an important cause for tumor recurrence and metastasis after surgery and has also become a potential clinical treatment target.[30] FZQX was produced by the Department of Pharmacy of Shanghai Municipal Hospital of TCM, consisting of 12 herbs, with the unique advantage of improving clinical symptoms, regulating immunity, enhancing chemotherapeutic drug sensitivity, and preventing recurrence and metastasis, and has been commonly used to treat lung cancer for 30 years.[31,32] This study explored the effect of FZQX on the proliferation and metastasis of human LUAD cells in vitro. The results showed that FZQX could significantly inhibit the number of clones of A549 and H1299 cells in a dose-dependent manner ($p < 0.05$, $p < 0.01$), increase the rate of early and late cell apoptosis ($p < 0.05$, $p < 0.01$), downregulate the expression of proliferation-related protein Ki67 and PNCA, and upregulate the expression of apoptosis-related protein Bax/Bcl-2 ($p < 0.05$, $p < 0.01$). The above results suggested that FZQX could exert antitumor effects by inhibiting cell proliferation and inducing apoptosis. In addition, the scratch test and Transwell assay showed that FZQX could significantly inhibit the migration and invasion of A549 and H1299 cells ($p < 0.05$, $p < 0.01$). Collectively, FZQX can significantly inhibit the proliferation and metastasis of human LUAD cells.

3.2. Mechanism of FZQX in Preventing the Recurrence of Postoperative Early-Stage LUAD. The oncogenesis or development is a complex regulatory network that is regulated under the interaction of multiple factors, including continuous proliferation signaling, induction of angiogenesis, activation of invasion and metastasis, abnormal cell metabolism, and escape from immune surveillance.[33] By integrating metabolomics and network pharmacology analysis, we found that FZQX could prevent recurrence and metastasis of postoperative early-stage LUAD, and the mechanism may be related to activating the receptor signal transduction pathway, inducing cell apoptosis, inhibiting aerobic glycolysis and rewiring tumor lipid metabolism reprogramming.

https://doi.org/10.1021/acsomega.3c00122
ACS Omega 2023, 8, 35555−35570

Tumor cell proliferation largely depends on three important pathways: protein kinase B (Akt), mitogen-activated protein kinase (MAPK), and mechanistic target of rapamycin (mTOR).[34−36] These pathways are mediated by many enzyme-linked receptors through signal transduction cascades to transfer growth, proliferation, and survival signals from the cell surface to the nucleus and, ultimately, lead to continuous cell proliferation. Receptor tyrosine kinases (RTKs) are the largest class of enzyme-linked receptors in cells. All RTKs are also receptors for various growth factors and enzymes that catalyze the phosphorylation of downstream target proteins. The signal transduction mediated by RTKs is closely related to cancer cell occurrence and development, so targeting RTKs would be a feasible antitumor treatment strategy.[37] In this study, the network pharmacology targets epidermal growth factor receptor (EGFR), threonine kinase B (Akt1), and sarcoma gene (SRC) are all members of the RTK family and are also key receptor proteins involved in tumor development. EGFR is a kind of proto-oncogene and is associated with tumor cell growth, metastasis, invasion, epithelial−mesenchymal transition (EMT), angiogenesis, drug resistance, immune regulation, and stem cell maintenance. Growing evidence suggests that EGFR causes different signal responses in cells through phosphorylation of cytoplasmic tyrosine kinase and binding with downstream signal pathways, including PI3K/AKT, JAK/STAT, and RAS/RAF/MAPK.[38−41] In addition, upon cancer initiation and formation, Akt mutation activates downstream signaling pathways, resulting in cancer immune tolerance and escape from classical immune attack.[42−44] Akt is a serine/threonine kinase of the AGC family, including the Akt1, Akt2, and Akt3 isoforms. Akt1 was initially found to be a proto-oncogene that plays an essential role in regulating various cell functions.[45] A large body of evidence has shown that Akt1 participates in the malignant progression of various solid tumors, promotes proliferation, and inhibits apoptosis.[46−49] Recent studies have also shown that the oncogene SRC promotes both cell death and cell proliferation through parallel pathways.[50]

Apoptosis is a kind of spontaneous and orderly death that is closely related to the production of oxygen free radicals, the disorder of cell energy metabolism, and the expression of caspase and B-lymphocyte tumor-2 (Bcl-2) family genes. The disorder of the apoptosis mechanism may induce the indefinite proliferation of malignant cells.[51] There are three main pathways of cell apoptosis, including the mitochondrial apoptotic pathway, endoplasmic reticulum pathway, and death receptor pathway. The mitochondrial pathway and endoplasmic reticulum stress are endogenous pathways, and the death receptor pathway is an exogenous pathway. Mitochondria play a central role in regulating the apoptotic pathway by releasing a large number of proapoptotic proteins.[52] In our network pharmacology analysis, Akt1 was a crucial component of the mitochondrial-mediated endogenous apoptosis pathway. Akt was reported to be located at the intersection of many mitochondrial-mediated apoptosis pathways and regulates apoptosis through phosphorylation of cell death factors.[53] A tremendous number of studies have shown that targeting Akt, as a monotherapy and a strategy used in combination with cytotoxicity and other targeted therapies, has been widely studied in the field of tumor therapy.[54] The experiment has proven that apatinib could effectively suppress the proliferation and induce the apoptosis of human gastric cancer HGC-27 cells, the mechanism of which was related to the inhibition of phosphorylation of the PI3K/Akt signaling pathway.[55] Similarly, kaempferol, a natural flavonoid, induced ROS-dependent apoptosis in pancreatic cancer cells via TGM2-mediated Akt/mTOR signaling.[56] By using network pharmacology analysis, we identified that FZQX induced apoptosis in LUAD cells and exerted antitumor effects via the PI3K/Akt signaling pathway.

Some studies have indicated that oncogenes are closely related to tumor metabolic reprogramming; thus, establishing the links between metabolic vulnerabilities and cancer genotypes might provide more effective treatment strategies.[57−59] The metabonomic analysis showed that 229 metabolites were significantly different between the pretreatment and control groups, of which 89 metabolites were regulated by FZQX, and these differential metabolites were mainly involved in cancer center carbon metabolism, glycerol phospholipid metabolism and the choline metabolism pathway. The pathways of cancer center carbon metabolism consist of the Embden−Meyerhof pathway (EMP) and pentose phosphate pathway (PPP). The "Warburg effect" is a characteristic metabolic mode of cancer. Even under aerobic conditions, cancer cells prioritize glycolysis to meet their unlimited proliferation.[60] Glucose is the main carbon source consumed by mammalian cells. In normal cells, glucose uptake is regulated by growth factors, while cancer cells usually absorb glucose from the extracellular environment to aid tumor development. On the one hand, genome amplification of RTK coding genes, such as EGFR, ERBB2, and c-Met, and mutation of PI3K, and its negative regulators PTEN and INPP4B enable cancer cells to take sufficient glucose independently, which maintains proliferation and promotes tumor progression. On the other hand, cancer cells acquire an aggressive phenotype and increase glucose uptake and glycolysis to promote cancer cell invasion.[61] In addition, the nonreceptor tyrosine kinase c-SRC encoded by the proto-oncogene SRC activates its enzyme activity by phosphorylating the PFKFB3 Tyr194 site and further catalyzes the allosteric activator F-2,6-BP of the key enzyme PFK1 of glycolysis, which promotes tumor cell proliferation and migration.[62]

In this research, the differentially expressed TOP20 genes were PS (18:1 (9Z)/20:5 (5Z,8Z,11Z,14Z,17Z)), PS (17:2 (9Z,12Z)/22:6 (4Z,7Z,10Z,13Z,16Z,19Z)), PA (12:0/18:4 (6Z,9Z,12Z,15Z)), PS (15:0/18:4 (6Z,9Z,12Z,15Z)), PC (16:0/00:0) [U], LysoPC (18Z: 1 (11Z)), LysoPC (18:0), and other lipid metabolism-related metabolites, and they were enriched in the glycerol phospholipid and choline metabolic pathways. Lipid metabolism disruption has been reported in several types of cancer. Metabolomic studies showed that in early-stage LUAD tissues, the expression of five lipids (phosphatidylcholines 16:0-18:1, 18:0-18:1, 18:0-18:2, 16:0-22:6, and 16:0-18:2) was increased, while three lipids (lysophosphatidylcholines 16:0, 18:0, and 20:4) were decreased.[63] Lysophosphatidic acid (LPA) is a downstream product of the lipid metabolite lysophosphatidylcholine (LPC) and a growth factor-like lipid signal molecule that combines with G protein-coupled receptors (GPCRs) on the cell membrane by paracrine or autocrine signaling and activates multiple downstream signaling pathways, including Rho/ROCK, AKT/mTOR, and Ras/MAPK, to regulate the progression of malignant tumors.[64] A recent study found that the proto-oncogene SRC could receive growth factors and obesity microenvironment-related factors such as insulin and leptin signals. By directly binding and phosphorylating lipin-1, which plays a major role in lipid metabolism, SRC enhances the catalytic activity of lipin-1 to synthesize glycerides, accelerates

https://doi.org/10.1021/acsomega.3c00122
ACS Omega 2023, 8, 35555−35570

the rate of glyceride synthesis, and then promotes the occurrence and development of breast cancer.[65] In addition, Akt phosphorylates serine 90 of phosphoenolpyruvate carboxyl kinase 1 (PCK1), leading to endoplasmic reticulum translocation of PCK1 and converting the original gluconeo metabolic enzyme function into a protein kinase function, which accelerates the cholesterol regulatory element binding protein (SREBP) signaling pathway and promotes the tumorigenesis of liver cancer.[66]

In addition, kinases related to lipid metabolites also play an important role in tumor invasion and metastasis. Diacylglycerol kinase alpha (DGKA) is a glycerol phospholipid metabolism-related kinase that can phosphorylate diacylglycerol to PA.[67] At the same time, DGKA, as an intercellular signal transduction molecule, activated multiple downstream signal pathways to widely participate in cell proliferation and differentiation, invasion and metastasis, metabolism, and other life activities by combining with PA binding proteins (PABPs) of the cell membrane in a paracrine or autocrine manner.[68,69] DGKA is not only highly expressed in some refractory malignant tumors, including melanoma, hepatocellular carcinoma, and glioblastoma cells but also has high abundance in T cells and induces T-cell response incompetence, which is the main mechanism to mediate the immune escape of advanced tumors.[70] Fu et al. showed that ritanserin, a small molecule inhibitor of DGKA, can synergistically enhance the anticancer effect of programmed cell death-1/programmed cell apoptosis ligand 1 block, while DGKA regulates the cell cycle and affects tumor growth by regulating the AKT/CDK signaling pathway.[69] Given the dual role of DGKA in T cells and tumor cells, DGKA-specific inhibitors are expected to become a dual effective anticancer treatment method and provide a promising new treatment strategy for refractory cancer. Autotaxin (ATX) is a secreted glycoprotein that can catalyze LPC to form LPA, which is further degraded by phospholipid phosphatases (PLPP). Studies have shown that the ATX-LPA axis is closely related to many pathological processes, such as inflammation, fibrosis, and metabolic diseases.[71,72] In tumors, the ATX-LPA axis is often in a highly active state. Targeting the ATX-LPA axis is a new strategy for the potential treatment of a variety of tumors, including non-small cell lung cancer.[73] The development of small molecule compounds targeting ATX has important scientific significance for promoting clinical transformation research.

3.3. Prospects for Future Research. In this study, network pharmacology combined with metabolomics was used to predict drug targets in a holistic manner. This method alters the TCM research model of "gene-targeted disease" and embodies the new model of "multiple genes, multiple targets and disease." The results showed that FZQX prescription has multicomponent, multitarget, and multichannel effects in preventing the recurrence of early-stage LUAD after surgery. It mainly plays an antirecurrence role in inhibiting the differentiation and proliferation of tumor cells, promoting apoptosis, and remodeling tumor metabolism. This method successfully predicted the main target and pathway of FZQX prescription to prevent the postoperative recurrence of early-stage LUAD for the first time, providing a basis for further study of the antitumor effect of FZQX prescription. The experimental scheme has an important reference value for research on compound drugs and is worthy of popularization and application in future research.

This study comprehensively analyzed the mechanism of FZQX in preventing the recurrence and metastasis of postoperative early-stage LUAD by integrated approaches; however, further research is still necessary. First, the pharmacodynamic basis of the antitumor effect of FZQX is still unclear. Second, this study was limited by the sample size of patients with postoperative early-stage LUAD, which may lead to false-positive results. Finally, network pharmacological prediction was based on an online network database, and further experimental validation is necessary to explore the antilung cancer mechanism. Based on the above points, future research will focus on a certain pathway to conduct cell and animal experiments and explore the mechanism by which FZQX prevents the recurrence and metastasis of postoperative early-stage LUAD.

4. CONCLUSIONS

In summary, our study demonstrated the mechanism of FZQX prescription in preventing the recurrence of postoperative early-stage LUAD based on metabolomics and network pharmacology. We obtained differential metabolites after treatment with FZQX by metabolomics, such as PS(18:1(9Z)/20:5-(5Z,8Z,11Z,14Z,17Z), PS(17:2(9Z,12Z)/22:6-(4Z,7Z,10Z,13Z,16Z,19Z)), PA(12:0/18:4(6Z,9Z,12Z,15Z)), PS(15:0/18:4(6Z,9Z,12Z,15Z)), PC(16:0/0:0)[U], LysoPC-(18:1(11Z)), and LysoPC(18:0), which are related to cancer central carbon metabolism, choline metabolism, and glycerol phospholipid metabolism signaling pathways. A total of 36 critical endogenous biomarkers of FZQX prescription were screened out by online database and network pharmacology, including KDR, ESR1, SRC, EGFR, and AKT, and these targets were enriched by the Ras signal pathway, PI3K/Akt signal pathway, and MAPK signal pathway. In summary, our results indicate that FZQX prevents the recurrence of postoperative early-stage LUAD by activating the receptor signal transduction pathway to inhibit proliferation, induce cell apoptosis, inhibit aerobic glycolysis, and reprogram tumor lipid metabolism.

5. MATERIALS AND METHODS

5.1. Components of FZQX Characterized by UPLC-Q-TOF/MS. *5.1.1. FZQX Preparation and Extraction.* In this system, the herbs HQ, BSS, MD, BZ, BFL, DS, SSB, SJC, SYQ, XKC, HZ, and ML (2:1:1:1:1:2:2:2:2:2:2:2:2) were soaked and decocted twice with 10 vol. of boiling water for 2 h and 5 vol. of boiling water for 35 min. The extraction solutions were filtered with a 150 mesh filter membrane, combined and then lyophilized. Next, 25 mL of 50% methanol was added to 0.3 g of FZQX lyophilized powder to obtain FZQX prescription methanol precipitation. After ultrasonic extraction for 30 min (250 W, 40 kHz) and centrifugation for 10 min (4 °C, 14,000 rpm·min^{-1}), the supernatant was used for UPLC-Q-TOF/MS analysis.

5.1.2. Analysis Condition. 5.1.2.1. Chromatographic Conditions. A Waters ACQUITY I-Class UPLC column (150 mm × 2.1 mm, 1.6 μm, Waters Corporation, Milford, MA, USA) was used to separate the aqueous extract of the standardized FZQX sample. 0.1% formic acid-water and acetonitrile were used as solvent A and solvent B of the optimal mobile phase, respectively. The gradient conditions were as follows: 0−2 min, 2% (B); 2−22 min, 2−60% (B); 22−24 min, 60−90% (B); 24−29 min, 90% (B); 29−30 min, 90−100% (B); 30−35 min, 100% (B). The column temperature was 35 °C, the injection volume was 2 μL, and the flow rate was set at 0.4 mL/min.

https://doi.org/10.1021/acsomega.3c00122
ACS Omega 2023, 8, 35555−35570

5.1.2.2. MS Conditions. MS experiments were executed on a UPLC-Q-TOF/MS equipped with an electrospray source ion (ESI). MS data were collected in both ESI+ and ESI− modes. The measurement parameters were as follows: capillary voltage 3 kV (ESI+) and 2.5 kV (ESI−), cracking voltage 120 V (ESI+) and taper hole voltage 40 V (ESI−), ion source temperature 120 °C, dry gas temperature 450 °C, conical hole gas flow rate 30 L/h (ESI+) and 50 L/h (ESI−), dry gas flow rate 600 L/h (ESI+) and 800 L/h (ESI−). The full scan mode was from m/z 50−1500, and the acquisition time was 0.1 s.

5.1.3. Data Processing. The data format of MS data was converted through MS convert software and was imported into MS-DIAL software for peak extraction and metabolite identification. MassLynx4.1 software (Waters Corporation, Milford, MA, USA) was used for data analysis for the accurate mass of fragment ions theory and mass spectral database.

5.2. Analysis of the Antitumor Mechanism of FZQX in Postoperative Early-Stage LUAD by a Network Pharmacology Approach. *5.2.1. Establishment of the Chemical Components Library of FZQX.* The chemical components of FZQX were collected according to the conditions under Section 5.1.2 to establish a chemical component library of FZQX.

5.2.2. Screening of Antitumor Targets for Components of FZQX. 5.2.2.1. Acquisition of Component Targets. To acquire the prediction target of the main components of FZQX, the chemical components were searched in the PubChem database[1] for the Canonical Simplified Molecular Input Line Entry System (SMILES) and were analyzed in the Swiss Target Prediction[2] to download the targets and common name. The targets and common names were converted into gene names corresponding to the GeneCards database[3] through the UniProt.[4]

5.2.2.2. Construction of Disease Targets. Cancer-related targets were searched in the treatment target database,[5] comparative genomic toxicology database and comparative toxicogenomics database[6] with the keyword "postoperative of early-stage lung adenocarcinoma." Among them, disease targets marked as "approved" or "marker/mechanism" were further screened. In the GeneCard database, we set the relevant targets with a relevance score >20 and used "postoperative of early-stage lung adenocarcinoma" as the keyword to find the relevant targets. Protein targets were converted into standard gene names through UniProt, and then the disease targets were integrated.

5.2.2.3. Acquisition of Direct Targets. The component targets and disease targets were imported into a Venn diagram online[7] to obtain component-disease intersection targets.

5.2.3. Protein−Protein Interaction Network Construction and Analysis. To establish the protein−protein interaction network (PPI network), the direct targets and indirect targets were imported into String.[8] The interaction network was visualized using Cytoscape 3.7.2 software.[9] The species was set as "*H. sapiens*," and the reliability was >0.9.

5.2.4. Gene Ontology and Kyoto Encyclopedia of Genes and Genomes Pathway Enrichment Analysis. Documents for molecular function, biological process, cellular components, and pathways were used to perform Gene Ontology (GO) enrichment analysis of the potential targets of postoperative early-stage LUAD after FZQX administration. The common targets were imported into the Omicshare[10] database with the species "*H. sapiens*," and a threshold of $p < 0.05$ was set for KEGG pathway enrichment analysis and GO bioprocess enrichment analysis.

5.3. Metabonomics Analysis of FZQX in Preventing Recurrence of Postoperative Early-Stage LUAD. *5.3.1. Patients and Clinical Data.* From January 2018 to March 2020, a total of 15 participants following surgical resection for early-stage LUAD and 10 healthy volunteers were recruited for the study. The study protocol was approved by the Ethics Committee of Shanghai Municipal Hospital of TCM affiliated with Shanghai University of TCM (2016SHL-KYYS-16). All patients signed informed consent forms, and this study was performed following the Declaration of Helsinki. The clinical trial was registered at the Chinese Clinical Trial Registry (ChiCTR-POC-16009499). The baseline clinical data of the enrolled patients and healthy control population are shown in Supplementary Table S5. The detailed diagnostic, inclusion, and exclusion criteria are described in Supplementary Material 1.

5.3.2. Sample Collection. The enrolled patients will receive the intervention of FZQX prescription. The specific drug components, medicinal parts, and dosages of FZQX prescriptions are listed in Supplementary Table S6. The FZQX granules were provided by the Department of Pharmacy of Shanghai Municipal Hospital of TCM affiliated with Shanghai University of TCM. Fully dissolve the granules by adding 200 mL boiling water each time. The patients in the treatment group were required to take FZQX prescription granules twice daily in the morning and evening 1 h after the meal. The course of treatment was 3 months. Venous blood samples (2 mL) from the healthy control, pretreatment, and posttreatment groups were collected into ethylenediaminetetraacetic acid anticoagulant tubes at 4 °C for 30 min, and then the samples were centrifuged at 12,000 rpm at 4 °C for 10 min. Afterward, the supernatant serum was transferred into new 1.5 mL Eppendorf tubes, and the sample information (name, number, type, and time) was marked. All samples were obtained by centrifugation and stored at −80 °C.

5.3.3. Sample Preparation. 5.3.3.1. Serum Sample Preparation. Serum samples were thawed at 4 °C on ice. Then, 100 μL of the sample was taken in an EP tube, extracted with 300 μL methanol acetonitrile mixture with a volume ratio of 2:1, treated with ultrasound for 10 min (during incubation in ice water), vortexed for 1 min, and then the samples were centrifuged at 13,000 rpm at 4 °C for 15 min, 30 μL supernatant was volatilized with nitrogen and resolved in 400 μL acetonitrile water mixture with a volume ratio of 1:4, and 150 μL supernatant was transferred into a fresh LC/MS glass vial.

5.3.3.2. Quality Control Sample Preparation. All samples from the control, pretreatment, and posttreatment groups were mixed in equal amounts to make quality control (QC) samples, and QC samples were prepared according to the method in Section 5.3.3.1.

5.3.4. Analysis Condition. 5.3.4.1. Chromatographic Conditions. An ACQUITY UPLC HSS T3 column (100 mm × 2.1 mm, 1.7 μm, Waters Corporation, Milford, MA, USA) was used to separate the aqueous extract of metabolomic samples. 0.1% formic acid-water and acetonitrile were used as solvent A and solvent B of the optimal mobile phase, respectively. The gradient conditions were as follows: 0−3 min, 4−30% B; 3−7 min, 30−37% B; 7−10 min, 37−60% B; 10−21 min, 60−100% B; 21−21.5 min, 100−100% B; 21.5−22.5 min, 100−4% B; 22.5−26 min, 4−4% B. The column temperature was 45 °C, the sample disk temperature was 4 °C, the injection volume was 5 μL, and the flow rate was set at 0.4 mL/min.

5.3.4.2. MS Conditions. MS experiments were executed on a UPLC-Q-TOF/MS equipped with an ESI. MS data were collected in both ESI+ and ESI− modes. The measurement parameters were as follows: positive and negative ion spray voltage 3.5 kV (ESI+) and 2.5 kV (ESI−), ionization source

https://doi.org/10.1021/acsomega.3c00122
ACS Omega 2023, 8, 35555−35570

voltage 4 kV, capillary voltage 35 V, and tube lens voltage 110 V. Both the sheath gas and the auxiliary gas were high-purity nitrogen (purity >99.99%), and the sheath gas and the auxiliary gas were 30 and 10 ARB, respectively. The normalized collision energy is 20, 30, and 40%. The full scan mode was from m/z 80−1000 and at 70,000 resolution.

5.3.5. Methodology and Test. 5.3.5.1. Instrument Precision. The same QC sample solution was injected continuously 6 times. The data are derived as the peak area. The relative standard deviation (RSD) value of each ion peak area was calculated. The ions with RSD <30% account for more than 80%.

5.3.5.2. Method Reproducibility. Six QC sample solutions were prepared in parallel for continuous injection analysis. The data were derived as peak areas. The RSD value of each ion peak area was calculated. The ions with RSD <30% accounted for more than 80%.

5.3.5.3. Sample Stability. The same QC sample solution was injected and analyzed at 6 time points in the whole injection sequence. The data were derived as the peak area, and the RSD value of each ion characteristic was calculated. The ions with RSD <30% account for more than 80%.

5.3.6. Data Processing. The LC/MS data were processed by using Progenesis QI (Version 2.3; Waters Corporation, Milford, MA, USA) for baseline filtering, peak identification, integration, retention time correction, peak alignment and normalization. The metabolomic profiling data were imported into Xcalibur (Version 4.2; Thermo Fisher Scientific, Waltham, MA, USA) for analysis and arrangement. The parameters were set as follows: mass deviation, $\delta \leq 5 \times 10^{-6}$. Information on excimer ion peaks and ion fragments obtained by MS was combined with a literature search and the Human Metabolome Database[11] to perform the metabolic comparison. The serum samples of each group were analyzed by principal component analysis (PCA) and partial least squares analysis (OPLS-DA) by using SIMCA software (Version 14.1; Umetrics AB, Umea, Vasterbotten, Sweden). After multivariate statistical analysis, only variables important in projection (VIP) > 1 and $p < 0.05$ were considered to be potential differential metabolites. The disturbed metabolites and enriched metabolic pathways were identified by the KEGG database.

5.4. Experimental Validation of FZQX Inhibition of LUAD Cell Proliferation and Metastasis In Vitro. *5.4.1. Cell Cultures.* The LUAD cell Lines H1299 and A549 were purchased from the Cell Bank of the Chinese Academy of Sciences (Shanghai, China). All cell lines were cultured in high sugar Dulbecco's modified Eagle medium (DMEM) (Gibco, Carlsbad, CA, USA) supplemented with 10% fetal bovine serum (FBS; Sigma−Aldrich Corp, St. Louis, MO, USA) and 1% penicillin−streptomycin (Thermo Fisher Scientific). All cell lines were stored in a cell culture incubator (Model 3111, Thermo Fisher Scientific) in the presence of 5% CO_2 at a temperature of 37 °C. Experiments were performed when the cells were in the logarithmic growth phase.

5.4.2. Drug Preparation. The composition of the FZQX prescription is shown in Supplementary Table S6. All Chinese herbal medicines were purchased from Jiangsu Jiangyin Tianjiang Pharmaceutical Co., Ltd. and authenticated by the pharmacy department of Shanghai Municipal Hospital of TCM affiliated with Shanghai University of TCM. Extraction of lyophilized powder of FZQX prescription: The herbs were soaked with 5 vol. of 75% ethanol overnight and decocted twice for 1 h and 45 min. The extraction solutions were filtered with a 0.22 μm filter membrane and then evaporated at 70 °C until a semisolid was formed. The concentration of the drug was diluted to 10 g/mL by DMEM complete medium and placed in the refrigerator at −20 °C for storage. UPLC-Q-TOF/MS analysis was used to control the quality of the lyophilized powder of the FZQX prescription.

5.4.3. Cell Counting Kit-8 Assay. Cell proliferation was detected by CCK-8 assay.[74] The cells were seeded in 96-well culture plates (Corning, NY, USA) at a density of 5×10^3 cells per well. Then the plates were divided into several groups treated with various concentrations of FZQX prescription (0, 2, 4, 6, 8, 10, 12, and 14 mg/mL) for 48 h. After incubation, the medium was replaced, and 10 μL CCK-8 reagent (Dojindo Chemical Laboratory, Kumamoto, Japan) was added to 100 μL FBS-free medium. After 1 h without light at 37 °C, the absorbance was determined by using a microplate reader (Model 3311, Thermo Fisher Scientific) at 450 nm. (Cell activity inhibition rate (%) = [(average OD value of the control group − average OD value of the experimental group)/(average OD value of the control group − average OD value of the blank group)] × 100%.)

5.4.4. Colony Formation Assay. The colony formation assay was performed as previously described.[75] The cells were plated into 6-well plates at a density of 1×10^3 cells per well, and 3 double holes were set up in each group. After incubation for 24 h, the cells were treated with FZQX at various drug concentration gradients, and the medium was changed two times weekly. After 14 days, the cells were treated in turn with 4% paraformaldehyde (Beyotime, Shanghai, China) for 30 min and crystal violet (Beyotime) for 20 min and were washed with phosphate-buffered saline (PBS; Corning, NY, USA) at least twice. The colonies were counted, and photographs were obtained through optical microscopy (Clone formation rate = number of clones/number of inoculated cells ×100%).

5.4.5. Apoptosis Analysis. Apoptosis assay was assessed by Annexin V-binding flow cytometry.[74] For flow cytometric analysis, cells were seeded in 6-well plates (2×10^4 cells/well) and treated with various concentrations of FZQX prescription for 48 h. Afterward, the cells were collected and stained with 2 μL Annexin V-FITC(Thermo Fisher Scientific) for 30 min and 2 μL propidium iodide (PI; Thermo Fisher Scientific) for 5 min in the dark according to the manufacturer's instructions. Finally, cell apoptosis was analyzed using FACSCanto flow cytometry (BD Biosciences, San Jose, CA, USA).

5.4.6. Western Blotting. Western blotting assays were performed as previously described.[74] Total protein was extracted from each group, and the protein concentration of each sample was measured by a BCA protein assay kit (Beyotime). The protein was transferred to a polyvinylidene fluoride (PVDF) membrane (Millipore, Bedford, MA, USA) and then blocked with 5% bovine serum albumin (BSA; Jackson ImmunoResearch Laboratories, West Grove, PA, USA) at room temperature for 120 min, followed by separate incubation with primary antibodies against Ki67, PCNA, Bax, Bcl-2, and β-actin (Cell Signaling Technology, Danvers, MA, USA) at 1:1000 overnight at 4 °C. The membranes were then probed with secondary antibodies (Cell Signaling Technology) at 1:3000 for 1 h. The intensity of each band was quantified by ImageJ Analysis software (National Institutes of Health, Bethesda, MD, USA) and normalized to the internal control β-actin. All experiments were performed in triplicate.

5.4.7. Scratch Wound Healing Assay. An in vitro invasion assay was performed as described previously.[76] A cluster of 2 ×

https://doi.org/10.1021/acsomega.3c00122
ACS Omega 2023, 8, 35555−35570

10^4 cells was seeded into 6-well plates and then cultured to 90% confluence. The confluent cell monolayer was wounded using a sterile 10 μL pipette tip. The suspended cells were washed three times with PBS, treated with various drug concentration gradients of FZQX in an FBS-free medium, and the control group was treated with the FBS-free medium. Then, photographs were taken at 0 and 48 h by optical microscopy. ImageJ Analysis software was used to evaluate migration distances. (Cell migration rate = $(A_{0h} - A_{48h})/A_{0h} \times 100\%$, where A_{0h} = the area of the wound measured immediately after scratching (t = 0); A_{48h} = the area of the wound measured after scratching (t = 48 h).)

5.4.8. Transwell Migration Assay. An in vitro migration assay was performed as described previously.[76] The Transwell migration assay was performed using chambers (Corning, NY, USA) and 6-well plates. The upper chamber with 100 μL serum-free medium contained 5×10^5 cells, while 500 μL medium with 10% serum was added to the lower chamber. Forty-eight hours later, the cells were fixed with 4% paraformaldehyde for 30 min at room temperature and subsequently stained with 0.1% crystal violet solution (Keygen Biotech Co., Jiangsu, China) for 30 min at 37 °C. Then, five fields were used to observe the cells that had penetrated the membrane, and pictures were taken under an optical microscope.

5.5. Statistical Analysis. Experimental data are reported as the mean ± standard deviation (SD) from at least three independent experiments. The statistical significance of differences between groups was analyzed with Student's t test. *p < 0.05 was considered to indicate statistical significance. Data analysis was performed using SPSS 24.0 software (IBM Corporation, Armonk, NY, USA).

■ ASSOCIATED CONTENT

Supporting Information

The Supporting Information is available free of charge at https://pubs.acs.org/doi/10.1021/acsomega.3c00122.

Diagnostic, Inclusion and Exclusion Criteria (Supplementary Material 1), the results of components targets (Table S1), the results of anti-cancer targets on online database (Table S2), the results of differential metabolites in the control vs pre-treatment group (Table S3), the results of differential metabolites in the pre-treatment vs post-treatment group (Table S4), the clinical data of enrolled patients and healthy control population (Table S5), drug composition of the FZQX prescription (Table S6) and diagnostic, inclusion and exclusion criteria (Material S1) (PDF)

■ AUTHOR INFORMATION

Corresponding Authors

Jianchun Wu − *Department of Oncology, Shanghai Municipal Hospital of Traditional Chinese Medicine, Shanghai University of Traditional Chinese Medicine, Shanghai 200071, China*; Email: eq219@126.com

Yan Li − *Department of Oncology, Shanghai Municipal Hospital of Traditional Chinese Medicine, Shanghai University of Traditional Chinese Medicine, Shanghai 200071, China*; Email: yan.xiaotian@shutcm.edu.cn

Authors

Yixi Zhang − *Department of Oncology, Shanghai Municipal Hospital of Traditional Chinese Medicine, Shanghai University of Traditional Chinese Medicine, Shanghai 200071, China*; orcid.org/0000-0003-0038-1467

Kai Ma − *Department of Oncology, Shanghai Municipal Hospital of Traditional Chinese Medicine, Shanghai University of Traditional Chinese Medicine, Shanghai 200071, China*

Lei Jiang − *Department of Thoracic Surgery, Shanghai Pulmonary Hospital, Tongji University School of Medicine, Shanghai 200433, China*

Lili Xu − *Department of Oncology, Shanghai Municipal Hospital of Traditional Chinese Medicine, Shanghai University of Traditional Chinese Medicine, Shanghai 200071, China*

Yingbin Luo − *Department of Oncology, Shanghai Municipal Hospital of Traditional Chinese Medicine, Shanghai University of Traditional Chinese Medicine, Shanghai 200071, China*

Complete contact information is available at: https://pubs.acs.org/10.1021/acsomega.3c00122

Author Contributions

Y.Z. and K.M. contributed equally to this work and were co-first authors. Conceptualization, Y.Z. and K.M.; methodology, Y.Z.; software, K.M.; validation, Y.Z. and K.M.; formal analysis, Y.Z. and K.M.; investigation, L.X; resources, Y.L.; data curation, K.M.; writing and original draft preparation, Y.Z.; writing and editing, Y.Z. and K.M.; visualization, Y.L.; supervision, J.W.; project administration, Y.L.; funding acquisition, Y.L. and J.W.; All authors have read and agreed to the published version of the manuscript.

Notes

The authors declare no competing financial interest.

■ ACKNOWLEDGMENTS

This research was financially supported by "the National Natural Science Fund of China [No. 81973795 and 82174183];"" the Pujiang Talent Plan, Shanghai [No. 2020PJD057]"; and "the Clinical Refwarch Plan of SHDC [No. SHDC2020CR4052].

■ ADDITIONAL NOTES

[1] https://pubchem.ncbi.nlm.Nih.gov/.
[2] http://www.swisstargetprediction.ch.
[3] http://www.genecards.org.
[4] https://www.uniprot.org.
[5] db.idrblab.net/.
[6] http://ctdbase.org/.
[7] https://bioinfogp.cnb.csic.es/tools/venny/
[8] https://Stringdb.org/.
[9] https://cytoscape.org/.
[10] http://www.omicshare.com/tools/index.php/
[11] HMDB, https://hmdb.ca.

■ REFERENCES

(1) Sung, H.; Ferlay, J.; Siegel, R. L.; Laversanne, M.; Soerjomataram, I.; Jemal, A.; Bray, F. Global Cancer Statistics 2020: GLOBOCAN Estimates of Incidence and Mortality Worldwide for 36 Cancers in 185 Countries. *CA, Cancer J. Clin.* **2021**, *71*, 209−249.

(2) Gillette, M. A.; Satpathy, S.; Cao, S.; Dhanasekaran, S. M.; Vasaikar, S. V.; Krug, K.; Petralia, F.; Li, Y.; Liang, W.; Reva, B.; Krek, A.; Ji, J.; Song, X.; Liu, W.; Hong, R.; Yao, L.; Blumenberg, L.; Savage, S. R.; Wendl, M. C.; Wen, B.; Li, K.; Tang, L. C.; MacMullan, M. A.; Avanessian, S. C.; Kane, M. H.; Newton, C. J.; Cornwell, M. I.; Kothadia, R. B.; Ma, W.; Yoo, S.; Mannan, R.; Vats, P.; Kumar-Sinha,

C.; Kawaler, E. A.; Omelchenko, T.; Colaprico, A.; Geffen, Y.; Maruvka, Y. E.; da Veiga Leprevost, F.; Wiznerowicz, M.; Gümüş, Z. H.; Veluswamy, R. R.; Hostetter, G.; Heiman, D. I.; Wyczalkowski, M. A.; Hiltke, T.; Mesri, M.; Kinsinger, C. R.; Boja, E. S.; Omenn, G. S.; Chinnaiyan, A. M.; Rodriguez, H.; Li, Q. K.; Jewell, S. D.; Thiagarajan, M.; Getz, G.; Zhang, B.; Fenyö, D.; Ruggles, K. V.; Cieslik, M. P.; Robles, A. I.; Clauser, K. R.; Govindan, R.; Wang, P.; Nesvizhskii, A. I.; Ding, L.; Mani, D. R.; Carr, S. A.; Webster, A.; Francis, A.; Charamut, A.; Paulovich, A. G.; Perou, A. M.; Godwin, A. K.; Karnuta, A.; Marrero-Oliveras, A.; Hindenach, B.; Pruetz, B.; Kubisa, B.; Druker, B. J.; Birger, C.; Jones, C. D.; Valley, D. R.; Rohrer, D. C.; Zhou, D. C.; Chan, D. W.; Chesla, D.; Clark, D. J.; Rykunov, D.; Tan, D.; Ponomareva, E. V.; Duffy, E.; Burks, E. J.; Schadt, E. E.; Bergstrom, E. J.; Fedorov, E. S.; Malc, E.; Wilson, G. D.; Chen, H. Q.; Krzystek, H. M.; Liu, H.; Culpepper, H.; Sun, H.; Zhang, H.; Day, J.; Suh, J.; Whiteaker, J. R.; Eschbacher, J.; McGee, J.; Ketchum, K. A.; Rodland, K. D.; Robinson, K.; Hoadley, K. A.; Suzuki, K.; Um, K. S.; Elburn, K.; Wang, L. B.; Chen, L.; Hannick, L.; Qi, L.; Sokoll, L. J.; Wojtyś, M.; Domagalski, M. J.; Gritsenko, M. A.; Beasley, M. B.; Monroe, M. E.; Ellis, M. J.; Dyer, M.; Burke, M. C.; Borucki, M.; Sun, M. H.; Roehrl, M. H.; Birrer, M. J.; Noble, M.; Schnaubelt, M.; Vernon, M.; Chaikin, M.; Krotevich, M.; Khan, M.; Selvan, M. E.; Roche, N.; Edwards, N. J.; Vatanian, N.; Potapova, O.; Grady, P.; McGarvey, P. B.; Mieczkowski, P.; Hariharan, P.; Madan, R.; Thangudu, R. R.; Smith, R. D.; Welsh, R. J.; Zelt, R.; Mehra, R.; Matteotti, R.; Mareedu, S.; Payne, S. H.; Cottingham, S.; Markey, S. P.; Chugh, S.; Smith, S.; Tsang, S.; Cai, S.; Boca, S. M.; Carter, S.; Gabriel, S.; de Young, S.; Stein, S. E.; Shankar, S.; Krubit, T.; Liu, T.; Skelly, T.; Bauer, T.; Velvulou, U.; Ozbek, U.; Petyuk, V. A.; Sovenko, V.; Bocik, W. E.; Maggio, W. W.; Chen, X.; Shi, Y.; Wu, Y.; Hu, Y.; Liao, Y.; Zhang, Z.; Shi, Z. Proteogenomic Characterization Reveals Therapeutic Vulnerabilities in Lung Adenocarcinoma. *Cell* **2020**, *182*, 200−225.e35.

(3) Butnor, K. J. Controversies and challenges in the histologic subtyping of lung adenocarcinoma. *Transl. Lung Cancer Res.* **2020**, *9*, 839−846.

(4) Gaikwad, A.; Souza, C. A.; Inacio, J. R.; Gupta, A.; Sekhon, H. S.; Seely, J. M.; Dennie, C.; Gomeset, M. M. Aerogenous metastases: a potential game changer in the diagnosis and management of primary lung adenocarcinoma. *AJR Am. J. Roentgenol.* **2014**, *203*, W570−W582.

(5) Ujiie, H.; Kadota, K.; Chaft, J. E.; Buitrago, D.; Sima, C. S.; Lee, M.; Huang, J.; Travis, W. D.; Rizk, N. P.; Rudin, C. M.; Jones, D. R.; Adusumilli, P. S. Solid predominant histologic subtype in resected stage I lung adenocarcinoma is an independent predictor of early, extrathoracic, multisite recur rence and of poor postrecurrence survival. *J. Clin. Oncol.* **2015**, *33*, 2877−2884.

(6) Horn, L.; Gettinger, S.; Camidge, D. R.; Smit, E. F.; Janjigian, Y. Y.; Miller, V. A.; Pao, W.; Freiwald, M.; Fan, J.; Wang, B.; Chand, V. K.; Groen, H. J. M. Continued use of afatinib with the addition of cetuximab after progression on afatinib in patients with EGFR mutation-positive non-small-cell lung cancer and acquired resistance to gefitinib or erlotinib. *Lung Cancer* **2017**, *113*, 51−58.

(7) Tsutani, Y.; Ito, M.; Shimada, Y.; Ito, H.; Ikeda, N.; Nakayama, H.; Okada, M. The impact of epidermal growth factor receptor mutation status on adjuvant chemotherapy for patients with high-risk stage I lung adenocarcinoma. *J. Thorac. Cardiovasc. Surg.* **2022**, *164*, 1306−1315.e4.

(8) Lv, J.; Jia, Y.; Li, J.; Kuai, W.; Li, Y.; Guo, F.; Xu, X.; Zhao, Z.; Lv, J.; Li, Z. Gegen Qinlian decoction enhances the effect of PD-1 blockade in colorectal cancer with microsatellite stability by remodelling the gut microbiota and the tumour microenvironment. *Cell Death Dis.* **2019**, *10*, 415.

(9) Li, C.; Chen, W.; Zhang, M.; Zhang, C.; Cao, B.; Dong, B.; Qi, S.; Zhang, Y.; Fei, X.; Li, X. Modulatory effects of Xihuang Pill on lung cancer treatment by an integrative approach. *Biomed. Pharmacother.* **2020**, *130*, No. 110553.

(10) Zhang, S.; Chen, W.; Wang, Y.; Wu, J.; Xu, L.; Yu, Y.; Tian, J.; Xu, R.; Fang, Z.; Jiang, L. Chinese Herbal Prescription Fu-Zheng-Qu-Xie Prevents Recurrence and Metastasis of Postoperative Early-Stage Lung Adenocarcinoma: A Prospective Cohort Study Followed with Potential Mechanism Exploration. *Oxid. Med. Cell. Longev.* **2021**, *2021*, No. 6673828.

(11) Liu, S.; Zhang, S.; Su, K.; Luo, Y.; Fang, Z.; Fang, Y. The effect of long-term traditional Chinese medicine treatment on disease-free survival of postoperative stage I-III lung cancer patients: a retrospective cohort study. *Tradit. Med. Res.* **2019**, *4*, 91−98.

(12) Yang, Q.; Wu, J.; Luo, Y.; Huang, N.; Zhen, N.; Zhou, Y.; Sun, F.; Li, Z.; Pan, Q.; Li, Y. (−)-Guaiol regulates RAD51 stability via autophagy to induce cell apoptosis in non-small cell lung cancer. *Oncotarget* **2016**, *7*, 62585−62597.

(13) Yang, X.; Zhu, J.; Wu, J.; Huang, N.; Cui, Z.; Luo, Y.; Sun, F.; Pan, Q.; Li, Y.; Yang, Q. (−)-Guaiol regulates autophagic cell death depending on mTOR signaling in NSCLC. *Cancer Biol. Ther.* **2018**, *19*, 706−714.

(14) Li, H.; Huang, N.; Zhu, W.; Wu, J.; Yang, X.; Teng, W.; Tian, J.; Fang, Z.; Luo, Y.; Chen, M.; Li, Y. Modulation the crosstalk between tumor-associated macrophages and non-small cell lung cancer to inhibit tumor migration and invasion by ginsenoside Rh2. *BMC Cancer* **2018**, *18*, 579.

(15) Chen, M.; Cheng, H.; Guo, Y.; Jiang, R.; Jiang, H.; Zhou, Y.; Fu, H.; Wu, M.; Zhang, X. Ophiopogonin B suppresses the metastasis and angiogenesis of A549 cells in vitro and in vivo by inhibiting the EphA2/Akt signaling pathway. *Oncol. Rep.* **2018**, *40*, 1339−1347.

(16) Lee, S.; Lee, S.; Roh, H. S.; Song, S. S.; Ryoo, R.; Pang, C. H.; Baek, K. H.; Kim, K. H. Cytotoxic Constituents from the Sclerotia of Poria cocos against Human Lung Adenocarcinoma Cells by Inducing Mitochondrial Apoptosis. *Cell* **2018**, *7*, 116.

(17) Feng, L.; Jia, X.; Shi, F.; Chen, Y. Identification of two polysaccharides from Prunella vulgaris L. and evaluation on their anti-lung adenocarcinoma activity. *Molecules* **2010**, *15*, 5093−5103.

(18) Liang, L.; Sun, F.; Wang, H.; Hu, Z. Metabolomics, metabolic flux analysis and cancer pharmacology. *Pharmacol. Ther.* **2021**, *224*, No. 107827.

(19) Xu, H.; Zhang, Y.; Wang, P.; Zhang, J.; Chen, H.; Zhang, L.; Du, X.; Zhao, C.; Wu, D.; Liu, F. A comprehensive review of integrative pharmacology-based investigation: A paradigm shift in traditional Chinese medicine. *Acta. Pharm. Sin. B* **2021**, *11*, 1379−1399.

(20) Huang, L.; Nie, L.; Dai, Z.; Dong, J.; Jia, X.; Yang, X.; Yao, L.; Ma, S. The application of mass spectrometry imaging in traditional Chinese medicine: a review. *Chin. Med.* **2022**, *17*, 35.

(21) Yi, T.; Zhu, L.; Tang, Y.; Zhang, J.; Liang, Z.; Xu, J.; Zhang, Z.; Yu, Z.; Bian, Z.; Yang, Z.; Chen, H. An integrated strategy based on UPLC−DAD−QTOF-MS for metabolism and pharmacokinetic studies of herbal medicines: Tibetan ″Snow Lotus″ herb (Saussurea laniceps), a case study. *J. Ethnopharmacol.* **2014**, *153*, 701−713.

(22) Chen, Q.; Zhu, L.; Tang, Y.; Kwan, H.; Zhao, Z.; Chen, H.; Yi, T. Comparative evaluation of chemical profiles of three representative 'snow lotus' herbs by UPLC-DAD-QTOF-MS combined with principal component and hierarchical cluster analyses. *Drug Test. Anal.* **2017**, *9*, 1105−1115.

(23) Tang, Y.; Pang, Y.; He, X.; Zhang, Y.; Zhang, J.; Zhao, Z.; Yi, T.; Chen, H. UPLC-QTOF-MS identification of metabolites in rat biosamples after oral administration of Dioscorea saponins: a comparative study. *J. Ethnopharmacol.* **2015**, *165*, 127−140.

(24) Feng, J.; Tang, Y.; Ji, H.; Xiao, Z.; Zhu, L.; Yi, T. Biotransformation of Dioscorea nipponica by Rat Intestinal Microflora and Cardioprotective Effects of Diosgenin. *Oxid. Med. Cell. Longev.* **2017**, *2017*, No. 4176518.

(25) Wang, X.; Lei, H.; Qi, X.; Guo, X.; Xu, X.; Zu, X.; Ye, J. Simultaneous determination of five bioactive components of XiaoJin Capsule in normal and mammary gland hyperplasia rat plasma using LC-MS/MS and its application to a pharmacokinetic study. *Biomed. Chromatogr.* **2021**, *35*, No. e5000.

(26) Newman, D. J. Modern traditional Chinese medicine: Identifying, defining and usage of TCM components. *Adv. Pharmacol.* **2020**, *87*, 113−158.

(27) Li, T.; Zhang, W.; Hu, E.; Sun, Z.; Li, P.; Yu, Z.; Zhu, X.; Zheng, F.; Xing, Z.; Xia, Z.; He, F.; Luo, J.; Tang, T.; Wang, Y. Integrated metabolomics and network pharmacology to reveal the mechanisms of

https://doi.org/10.1021/acsomega.3c00122
ACS Omega 2023, 8, 35555−35570

hydroxysafflor yellow A against acute traumatic brain injury. *Comput. Struct. Biotechnol. J.* **2021**, *19*, 1002−1013.
(28) Li, L.; Dai, W.; Li, W.; Zhang, Y.; Wu, Y.; Guan, C.; Zhang, A.; Huang, H.; Li, Y. Integrated Network Pharmacology and Metabonomics to Reveal the Myocardial Protection Effect of Huang-Lian-Jie-Du-Tang on Myocardial Ischemia. *Front. Pharmacol.* **2021**, *11*, No. 589175.
(29) Qu, Y.; Aly, R. G.; Takahashi, Y.; Adusumilli, P. S. Micropapillary lung adenocarcinoma and micrometastasis. *J. Thorac. Dis.* **2017**, *9*, 3443−3446.
(30) Su, Z.; Wang, Z.; Ni, X.; Duan, J.; Gao, Y.; Zhuo, M.; Li, R.; Zhao, J.; Ma, Q.; Bai, H.; Chen, H.; Wang, S.; Chen, X.; An, T.; Wang, Y.; Tian, Y.; Yu, J.; Wang, D.; Xie, X. S.; Bai, F.; Wang, J. Inferring the Evolution and Progression of Small-Cell Lung Cancer by Single-Cell Sequencing of Circulating Tumor Cells. *Clin. Cancer Res.* **2019**, *25*, 5049−5060.
(31) Liu, S.; Zhang, S.; Luo, Y.; Fang, Z.; Fang, Y. Retrospective cohort study of Fuzheng Quxie prescription on improving progression-free survival of lung cancer patients. *Acta Chin. Med.* **2019**, *34*, 1497−1501.
(32) Xu, L.; Zhang, S.; Wang, Y.; Luo, Y.; Fang, Z.; Fang, Y.; Xu, R.; Guo, P.; Wu, J.; Li, Y. The Efficacy of Long-Term Chinese Herbal Medicine Use on Lung Cancer Survival Time: A Retrospective Two-Center Cohort Study with Propensity Score Matching. *Evid. Based Complement Alternat. Med.* **2021**, *2021*, No. 5522934.
(33) Hanahan, D.; Weinberg, R. A. Hallmarks of cancer:the next generation. *Cell* **2011**, *144*, 646−674.
(34) Song, M.; Bode, A. M.; Dong, Z.; Lee, M. AKT as a Therapeutic Target for Cancer. *Cancer Res.* **2019**, *79*, 1019−1031.
(35) Wei, J.; Liu, R.; Hu, X.; Liang, T.; Zhou, Z.; Huang, Z. MAPK signaling pathway-targeted marine compounds in cancer therapy. *J. Cancer Res. Clin. Oncol.* **2021**, *147*, 3−22.
(36) Mossmann, D.; Park, S.; Hall, M. N. mTOR signalling and cellular metabolism are mutual determinants in cancer. *Nat. Rev. Cancer* **2018**, *18*, 744−757.
(37) Du, Z.; Lovly, C. M. Mechanisms of receptor tyrosine kinase activation in cancer. *Mol. Cancer* **2018**, *17*, 58.
(38) Sigismund, S.; Avanzato, D.; Lanzetti, L. Emerging functions of the EGFR in cancer. *Mol. Oncol.* **2018**, *12*, 3−20.
(39) Sabbah, D. A.; Hajjo, R.; Sweidan, K. Review on Epidermal Growth Factor Receptor (EGFR) Structure, Signaling Pathways, Interactions, and Recent Updates of EGFR Inhibitors. *Curr. Top. Med. Chem.* **2020**, *20*, 815−834.
(40) Liu, Q.; Yu, S.; Zhao, W.; Qin, S.; Chu, Q.; Wu, K. EGFR-TKIs resistance via EGFR-independent signaling pathways. *Mol. Cancer* **2018**, *17*, 53.
(41) Janecka-Widła, A.; Majchrzyk, K.; Mucha-Małecka, A.; Biesaga, B. EGFR/PI3K/Akt/mTOR pathway in head and neck squamous cell carcinoma patients with different HPV status. *Pol. J. Pathol.* **2021**, *72*, 296−314.
(42) Revathidevi, S.; Munirajan, A. K. Akt in cancer: Mediator and more. *Semin. Cancer Biol.* **2019**, *59*, 80−91.
(43) Hua, H.; Zhang, H.; Chen, J.; Wang, J.; Liu, J.; Jiang, Y. Targeting Akt in cancer for precision therapy. *J. Hematol. Oncol.* **2021**, *14*, 128.
(44) Fattahi, S.; Amjadi-Moheb, F.; Tabaripour, R.; Ashrafi, G. H.; Akhavan-Niaki, H. PI3K/AKT/mTOR signaling in gastric cancer: Epigenetics and beyond. *Life Sci.* **2020**, *262*, No. 118513.
(45) Degan, S. E.; Gelman, I. H. Emerging Roles for AKT Isoform Preference in Cancer Progression Pathways. *Mol. Cancer Res.* **2021**, *19*, 1251−1257.
(46) Zhang, X.; Wang, S.; Wang, H.; Cao, J.; Huang, X.; Chen, Z. Circular RNA circNRIP1 acts as a microRNA-149-5p sponge to promote gastric cancer progression via the AKT1/mTOR pathway. *Mol. Cancer* **2019**, *18*, 20.
(47) Herberts, C.; Murtha, A. J.; Fu, S.; Wang, G.; Schönlau, E.; Xue, H.; Lin, D.; Gleave, A.; Yip, S.; Angeles, A.; Hotte, S.; Tran, B.; North, S.; Taavitsainen, S.; Beja, K.; Vandekerkhove, G.; Ritch, E.; Warner, E.; Saad, F.; Iqbal, N.; Nykter, M.; Gleave, M. E.; Wang, Y.; Annala, M.; Chi, K. N.; Wyatt, A. W. Activating AKT1 and PIK3CA Mutations in Metastatic Castration-Resistant Prostate Cancer. *Eur. Urol.* **2020**, *78*, 834−844.
(48) George, B.; Gui, B.; Raguraman, R.; Paul, A. M.; Nakshatri, H.; Pillai, M. R. AKT1 Transcriptomic Landscape in Breast Cancer Cells. *Cell* **2022**, *11*, 2290.
(49) Xu, Z.; Xu, M.; Liu, P.; Zhang, S.; Shang, R.; Qiao, Y.; Che, L.; Ribback, S.; Cigliano, A.; Evert, K.; Pascale, R. M.; Dombrowski, F.; Evert, M.; Chen, X.; Calvisi, D. F.; Chen, X. The mTORC2-Akt1 Cascade Is Crucial for c-Myc to Promote Hepatocarcinogenesis in Mice and Humans. *Hepatology* **2019**, *70*, 1600−1613.
(50) Nishida, H.; Okada, M.; Yang, L.; Takano, T.; Tabata, S.; Soga, T.; Ho, D. M.; Chung, J.; Minami, Y.; Yoo, S. Methionine restriction breaks obligatory coupling of cell proliferation and death by an oncogene Src in Drosophila. *Elife* **2021**, *10*, No. e59809.
(51) Wong, R. S. Y. Apoptosis in cancer: from pathogenesis to treatment. *J. Exp. Clin. Cancer Res.* **2011**, *30*, 87.
(52) Das, S.; Shukla, N.; Singh, S. S.; Kushwaha, S.; Shrivastava, R. Mechanism of interaction between autophagy and apoptosis in cancer. *Apoptosis* **2021**, *26*, 512−533.
(53) Singh, P.; Lim, B. Targeting Apoptosis in Cancer. *Curr. Oncol. Rep.* **2022**, *24*, 273−284.
(54) Shariati, M.; Meric-Bernstam, F. Targeting AKT for cancer therapy. *Expert Opin. Investig. Drugs* **2019**, *28*, 977−988.
(55) Jia, X.; Wen, Z.; Sun, Q.; Zhao, X.; Yang, H.; Shi, X.; Xin, T. Apatinib suppresses the Proliferation and Apoptosis of Gastric Cancer Cells via the PI3K/Akt Signaling Pathway. *J. BUON* **2019**, *24*, 1985−1991.
(56) Wang, F.; Wang, L.; Qu, C.; Chen, L.; Geng, Y.; Cheng, C.; Yu, S.; Wang, D.; Yang, L.; Meng, Z. Kaempferol induces ROS-dependent apoptosis in pancreatic cancer cells via TGM2-mediated Akt/mTOR signaling. *BMC Cancer* **2021**, *21*, 396.
(57) Martinez-Reyes, I.; Chandel, N. S. Cancer metabolism: looking forward. *Nat. Rev. Cancer* **2021**, *21*, 669−680.
(58) Parida, P. K.; Marquez-Palencia, M.; Nair, V.; Kaushik, A. K.; Kim, K.; Sudderth, J.; Quesada-Diaz, E.; Cajigas, A.; Vemireddy, V.; Gonzalez-Ericsson, P. I.; Sanders, M. E.; Mobley, B. C.; Huffman, K.; Sahoo, S.; Alluri, P.; Lewis, C.; Peng, Y.; Bachoo, R. M.; Arteaga, C. L.; Hanker, A. B.; DeBerardinis, R. J.; Malladi, S. Metabolic diversity within breast cancer brain-tropic cells determines metastatic fitness. *Cell Metab.* **2022**, *34*, 90−105.e7.
(59) Du, J.; Su, Y.; Qian, C.; Yuan, D.; Miao, K.; Lee, D.; Ng, A. H. C.; Wijker, R. S.; Ribas, A.; Levine, R. D. Raman-guided subcellular pharmaco-metabolomics for metastatic melanoma cells. *Nat. Commun.* **2020**, *11*, 4830.
(60) Vitale, I.; Shema, E.; Loi, S.; Galluzzi, L. Intratumoral heterogeneity in cancer progression and response to immunotherapy. *Nat. Med.* **2021**, *27*, 212−224.
(61) Ran, C.; Liu, H.; Hitoshi, Y.; Israel, M. A. Proliferation-independent control of tumor glycolysis by PDGFR-mediated AKT activation. *Cancer Res.* **2013**, *73*, 1831−1843.
(62) Ma, H.; Zhang, J.; Zhou, L.; Wen, S.; Tang, H.; Jiang, B.; Zhang, F.; Suleman, M.; Sun, D.; Chen, A.; Zhao, W.; Lin, F.; Tsau, M. T.; Shih, L. M.; Xie, C.; Li, X.; Lin, D.; Hung, L. M.; Cheng, M. L.; Li, Q. c-Src Promotes Tumorigenesis and Tumor Progression by Activating PFKFB3. *Cell Rep.* **2020**, *30*, 4235−4249.e6.
(63) Wang, G.; Qiu, M.; Xing, X.; Zhou, J.; Yao, H.; Li, M.; Yin, R.; Hou, Y.; Li, Y.; Pan, S. Lung cancer scRNA-seq and lipidomics reveal aberrant lipid metabolism for early-stage diagnosis. *Sci. Transl. Med.* **2022**, *14*, No. eabk2756.
(64) Lin, Y.; Lin, Y.; Chen, C. Lysophosphatidic Acid Receptor Antagonists and Cancer: The Current Trends, Clinical Implications, and Trials. *Cell* **2021**, *10*, 1629.
(65) Song, L.; Liu, Z.; Hu, H.; Yang, Y.; Li, T.; Lin, Z.; Ye, J.; Chen, J.; Huang, X.; Liu, D. Proto-oncogene Src links lipogenesis via lipin-1 to breast cancer malignancy. *Nat. Commun.* **2020**, *11*, 5842.
(66) Xu, D.; Wang, Z.; Xia, Y.; Shao, F.; Xia, W.; Wei, Y.; Li, X.; Xu, Q.; Lee, J. H.; Du, L. The gluconeogenic enzyme PCK1 phosphorylates INSIG1/2 for lipogenesis. *Nature* **2020**, *580*, 530−535.

https://doi.org/10.1021/acsomega.3c00122
ACS Omega 2023, 8, 35555−35570

(67) Goto, K.; Hozumi, Y.; Kondo, H. Diacylglycerol, phosphatidic acid, and the converting enzyme, diacylglycerol kinase, in the nucleus. *Biochim. Biophys. Acta* **2006**, *1761*, 535−541.
(68) Fumio, S.; Fumi, H.; Masayuki, E.; Sakai, H.; Takahashi, D. The Roles of Diacylglycerol kinase α in Cancer Cell Proliferation and Apoptosis. *Cancers* **2021**, *13*, 5190.
(69) Takeishi, K.; Taketomi, A.; Shirabe, K.; Toshima, T.; Motomura, T.; Ikegami, T.; Yoshizumi, T.; Sakane, F.; Maehara, Y. Diacylglycerol kinase alpha enhances hepatocellular carcinoma progression by activation of Ras-Raf-MEK-ERK pathway. *J. Hepatol.* **2012**, *57*, 77−83.
(70) Marchan, R.; Buttner, B.; Lambert, J.; Edlund, K.; Glaeser, I.; Blaszkewicz, M.; Leonhardt, G.; Marienhoff, L.; Kaszta, D.; Anft, M. Glycerol-3-phosphate Acyltransferase 1 Promotes Tumor Cell Migration and Poor Survival in Ovarian Carcinoma. *Cancer Res.* **2017**, *77*, 4589−4601.
(71) Liu, S.; Murph, M.; Panupinthu, N.; Mills, G. ATX-LPA Receptor Axis in Inflammation and Cancer. *Cell Cycle* **2009**, *8*, 3695−3701.
(72) Zhang, G.; Cheng, Y.; Zhang, Q.; Li, X.; Zhou, J.; Wang, J.; Wei, L. ATX-LPA axis facilitates estrogen-induced endometrial cancer cell proliferation via MAPK/ERK signaling pathway. *Mol. Med. Rep.* **2018**, *17*, 4245−4252.
(73) Magkrioti, C.; Oikonomou, N.; Kaffe, E.; Mouratis, M.; Xylourgidis, N.; Barbayianni, I.; Megadoukas, P.; Harokopos, V.; Valavanis, C.; Chun, J.; Kosma, A.; Stathopoulos, G.; Bouros, E.; Bouros, D.; Syrigos, K.; Aidinis, V. The Autotaxin-Lysophosphatidic Acid Axis Promotes Lung Carcinogenesis. *Cancer Res.* **2018**, *78*, 3634−3644.
(74) Que, Z.; Zhou, Z.; Luo, B.; Dong, C.; Jiang, Y.; Li, H.; Tian, J. Jingfukang induces anti-cancer activity through oxidative stress-mediated DNA damage in circulating human lung cancer cells. *BMC Complement Altern. Med.* **2019**, *19*, 204.
(75) Que, Z.; Luo, B.; Wang, C.; Qian, F.; Jiang, Y.; Li, Y.; Han, X.; Li, H.; Liu, J.; Tian, J. Proteomics analysis of tumor exosomes reveals vital pathways of Jinfukang inhibiting circulating tumor cells metastasis in lung cancer. *J. Ethnopharmacol.* **2020**, *256*, No. 112802.
(76) Liang, X.; Chen, W.; Shi, H.; Gu, X.; Li, Y.; Qi, Y.; Xu, K.; Zhao, A.; Liu, J. PTBP3 contributes to the metastasis of gastric cancer by mediating CAV1 alternative splicing. *Cell. Death Dis.* **2018**, *9*, 569.

https://doi.org/10.1021/acsomega.3c00122
ACS Omega 2023, 8, 35555−35570